Applied Thermal Engineering 278 (2025) 127174

Contents lists available at ScienceDirect

Applied Thermal Engineering

journal homepage: www.elsevier.com/locate/apthermeng

Research Paper

CFD analysis of twin turbulent plane jets confined by walls: Effects of geometry on flow dynamics and heat transfer

Francisco Zdanowski [a,b,*], Isabel Malico [a,b,c]

[a] Universidade de Évora, Escola de Ciências e Tecnologia, Departamento de Eng.ª Mecatrónica, R. Romão Ramalho 59, 7000-671 Évora, Portugal

[b] IDMEC, Instituto Superior Técnico, Universidade de Lisboa, Av. Rovisco Pais 1, 1049-001 Lisboa, Portugal

[c] Complex Flow Systems Lab (CFS Lab), Institute of Earth Sciences, R. Romão Ramalho 59, 7000-671 Évora, Portugal

ARTICLE INFO

Keywords:
Computational fluid dynamics
Reynolds-averaged Navier-Stokes models
Turbulence models
Offset jet
Dual offset jet
Parallel jets

ABSTRACT

This study investigates the flow and heat transfer behavior of heated twin turbulent plane parallel jets confined between isothermal walls. The focus is on understanding the impact of key geometric parameters: the separation ratio and offset ratio. While dual plane offset jets have been studied in various unconfined or isothermal configurations, the combined impact of heating, confinement and jet geometry remains insufficiently addressed in the literature. This work fills the gap by conducting a systematic analysis using two-dimensional Computational Fluid Dynamics simulations. Validation against experimental data for three different jet configurations showed good agreement with experimental data, with the SST k-ω model providing the most balanced performance out of four turbulent models tested. The results revealed that despite geometrical symmetry, the jets consistently deflect towards one of the walls due to the Coandă effect, leading to flow asymmetry and influencing heat transfer. An increase in the separation and offset ratios shifts the reattachment point downstream, weakens the intensity of wall impingement, and reduces local peak wall shear stress and the maximum local Nusselt number at the walls. Increasing the offset ratio from 2 to 5 enhanced average heat transfer at the jet impingement wall by 20%. Conversely, increasing the separation ratios from 2 to 5 decreased the average heat transfer to the opposite wall by 11% and to the impingement wall by 1%. These findings contribute to a better understanding of complex wall-jet interactions and support the design of thermal systems involving confined turbulent dual offset jets.

1. Introduction

Turbulent plane parallel jets confined by walls are common in many engineering and environmental systems where efficient flow control, mixing, and heat transfer are essential. These systems include combustion reactors, industrial mixing devices, electronic cooling systems, ventilation systems, propulsion technologies, pollution control systems, and heat transfer enhancement systems in industrial equipment [1–3]. Despite their practical relevance, the flow and thermal behavior of confined plane parallel jets have not been systematically studied, particularly in terms of how geometric parameters affect flow and heat transfer. Understanding the behavior of these flows is essential for optimizing system performance, and achieving efficient design and proper functioning in a wide range of applications.

Two plane parallel jets can interact through entrainment and shear-layer merging. While numerous studies have investigated these interactions in unconfined configurations, revealing key phenomena such as merging distances and velocity decay [4–7], the presence of confining walls parallel to the nozzle axes significantly increases the complexity of the flow. These walls limit jet spreading and introduce wall-induced effects. Depending on the initial conditions and geometric configuration, the jets may merge or remain distinct [8]. Additionally, the Coandă effect can cause jets to deflect towards adjacent walls, influencing flow stability, mixing efficiency, and wall shear stress [3,9,10]. When a jet is released from a height, parallel to a flat surface, the proximity of the surface creates a low-pressure region on the side near the surface due to the interaction of the jet with the boundary and the entrainment of surrounding fluid. The pressure difference between the surface side and the side away from the surface causes the jet to deflect towards the surface. As a result, the jet impinges on the surface. If the jet is unventilated, part of the fluid is deflected upstream of the reattachment point and the other part downstream. As a consequence, in the region between the jet exit and the point of reattachment, a recirculation zone typically forms. Downstream of the impingement point, the fluid flows along the

* Corresponding author.
E-mail addresses: zdanowski@uevora.pt (F. Zdanowski), imbm@uevora.pt (I. Malico).

https://doi.org/10.1016/j.applthermaleng.2025.127174
Received 7 March 2025; Received in revised form 3 June 2025; Accepted 7 June 2025
Available online 12 June 2025

solid boundary and, further downstream, develops into a wall jet flow.

Previous research has extensively explored the behavior of turbulent plane jets near walls, with early investigations focusing on single-jet configurations. Both experimental (e.g., [10–15]) and numerical (e.g., [15–17]) studies provide valuable insights into the flow dynamics of offset jets – jets discharged at a certain height above a wall parallel to the nozzle axis. Experimental investigations have revealed important characteristics of offset jet features such as recirculation zones near the wall, jet deflection, and reattachment points [11,12,15]. Some of the studies on offset jets have demonstrated that the offset distance between the nozzle and the wall significantly influences the flow structure, particularly the size of the recirculation region [11,13,16]. It has also been shown that the flow becomes independent of nozzle Reynolds numbers beyond a certain threshold [11].

Even though the hydrodynamics of offset jet flows has been extensively researched, non-isothermal offset jet flows have received less attention. Experimental (e.g., [18–21]) and numerical (e.g., [22,23]) studies have analyzed various offset wall boundary conditions, including adiabatic [18,22], constant wall temperature [24], and constant heat flux [19,23]. It has been observed that, for an adiabatic impingement wall, the thermal energy in the recirculation region remains relatively uniform for both low and high offset ratios, with the temperature close to the impinging temperature but varying with the offset ratio, especially near the wall [18]. Additionally, for an adiabatic wall, the maximum Nusselt number nearly coincides with the reattachment point, its magnitude and position being well correlated with the offset distance [19,23].

Research on double jet flows over horizontal plates has primarily focused on the dual jet configuration, which combines an offset jet with a wall jet (a jet discharged tangential to a wall). Experimental (e.g., [25,26]) and numerical studies (e.g., [27–29]) have described the complex flow interactions between the jets, and between the jets and the wall. For relatively small separation distances between nozzles, periodic vortex shedding occurs [25], while greater separations lead to steady flow patterns [28]. Mondal et al. [28] observed the development of a von Kármán vortex street for separation ratios between 0.7 and 2.1, with steady flow outside this range. A commonly used turbulence modelling approach for studying dual jets is solving the Reynolds-averaged Navier-Stokes equations (RANS) [30], typically using the standard k-ε turbulence model [28,29]. Recent studies reinforce that jet spacing strongly influences the size of the recirculation, the jet deflection, and the location of the merging point downstream [3].

The thermal behavior of dual jets has also received attention. Early studies examined the effects of jet spacing [31,32], Reynolds number [31,33], inlet velocity ratio [31], and thermal wall boundary conditions [33] using various turbulence models. More recent investigations have continued to explore these parameters using both experimental and numerical approaches, further confirming their significance in determining local and surface-averaged Nusselt numbers [34–38]. Collectively, the studies highlight the sensitivity of heat transfer in dual jet systems to jet spacing, Reynolds number, and wall boundary conditions, with consistent trends observed across a range of turbulence models.

Studies involving two offset jets (both jets are discharged at a certain height above a wall) remain limited. Mondal and Pramanik [39] conducted a numerical investigation of the mean flow and turbulence characteristics of isothermal dual offset jets. Their study provides insights on the flow interactions between two offset jets, which significantly influence the reattachment phenomenon. The study highlights the critical role of the separation distance between the jets in determining flow structures, such as the size and intensity of recirculation zones. These authors followed the RANS approach and used the standard k-ε turbulence model. Mondal and O'Shaughnessy [40] later investigated the conjugate heat transfer characteristics of turbulent dual offset jets interacting with a heated solid wall, revealing that the non-dimensional temperature and heat flux profiles at the fluid–solid interface are influenced by Reynolds number, Prandtl number, thermal conductivity ratio, and wall thickness. The findings highlight the need for further research into heated twin offset jets.

Characterized by their complex flow behavior, including recirculation zones, and significant velocity gradients, confined parallel jets present a challenging test case for validating numerical models and model accuracy. Computational Fluid Dynamics (CFD) has proven to be a valuable tool for simulating jet flows, offering insights into the underlying physics without the need for costly experimental setups [15,41], making it a valuable approach to study non-isothermal confined parallel jets. The choice of an appropriate turbulence model is a crucial aspect of CFD simulations of confined parallel jets, where interactions between jets and boundary surfaces introduce complex flow separation and mixing. Among turbulence modeling approaches, Reynolds-averaged Navier-Stokes models, such as k-ε and k-ω, are widely used in the simulation of single and dual offset jets due to their computational efficiency [15–17,22,40]. Given the high computational cost of more advanced turbulence modelling approaches, RANS remains a practical and widely accepted method for studying the heat transfer and flow characteristics of jets [17].

This study addresses the limited research on confined, heated, twin turbulent plane parallel jets. Both jets are offset from walls parallel to the nozzle axes and have equal streamwise exit velocities. The flow is modelled using CFD under two-dimensional, incompressible and turbulent conditions. The study systematically explores the influence of two key geometric parameters: the ratio of the distance between nozzles to the jet widths ($s/w \in [2,5]$) and the ratio of the distance between the wall and the nozzles to the jet width ($h/w \in [2,5]$). The model used in this study is validated against experimental results for three test cases: a turbulent plane offset jet [9,10], a heated turbulent plane offset jet [18] and twin plane turbulent isothermal free jets [6]. These cases are also used to systematically compare the performance of various turbulence models in predicting the flow characteristics of jet flows with features similar to the configuration under investigation. By comparing the results from these models with experimental data, this paper evaluates their accuracy and suitability for simulating two-dimensional confined parallel jet flows.

The significance of this study lies in its focus on confined, heated, twin plane parallel jets — a configuration with high practical relevance but limited prior investigation. To the best of the authors' knowledge, this is the first systematic study to examine the combined effects of offset and separation ratios on both flow dynamics and heat transfer in such a setting. The results offer new insights into the understanding of confined turbulent plane parallel jets, particularly in heated flows with complex interactions between jets and solid boundaries. By systematically examining the effects of key geometric parameters on flow dynamics and heat transfer, the study provides valuable insights for optimizing engineering systems that utilize confined parallel jets. Moreover, the validation and evaluation of turbulence models against experimental data offer critical guidance for selecting appropriate numerical approaches in future studies, improving the reliability and efficiency of CFD simulations for similar configurations. These contributions address a significant gap in the literature and pave the way for improved design and performance of systems involving confined parallel jets.

2. Methods

2.1. Problem description

Fig. 1 presents the configuration of the confined twin parallel jets analyzed in this study. Two heated plane incompressible turbulent air jets with the same streamwise exit velocity are discharged from identical nozzles into still ambient air at 25 °C confined by walls. The nozzles, with width w, are a distance s apart from each other and their axes are both offset by a distance $h + w/2$ from the nearest wall (top or bottom). The width of the nozzle is kept constant (30.5 mm), but the separation ratio (s/w) and the offset ratio (h/w) of the two jets were varied to

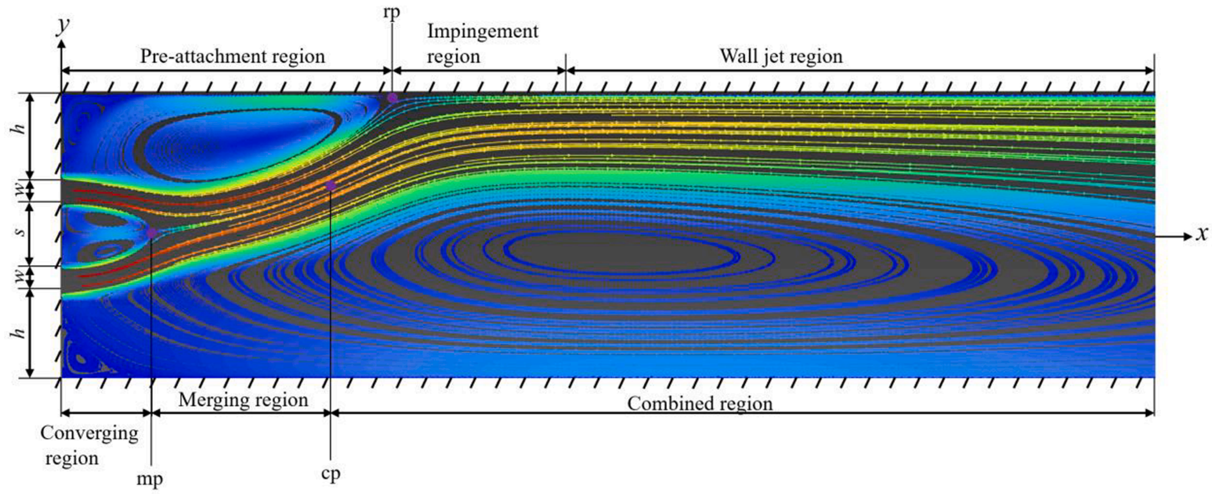

Fig. 1. Confined twin parallel jet analyzed.

analyze the influence of these parameters on the flow behavior and heat transfer characteristics. The jets are discharged at $T_0 = 100$ °C and the Reynolds number based on the nozzle width and exit velocity, *Re*, is kept constant and equal to 15000. The origin of the coordinate system is located at the intersection of the vertical left wall and the centerline between the two horizontal walls. (x and y are, respectively, the axes along that centerline and along the left wall). The length of the domain perpendicular to the x-y plane is large enough so that the flow can be considered two-dimensional.

The flow can be divided into several regions. Under specific conditions, after being discharged, the inner shear layers of the two jets interact and merge. The merge point (mp) is a free stagnation point where the mean velocity is zero, and the region between the nozzle exit plane and the merge point is called the converging region. Downstream of the merge point, the two jets continue to interact in the so-called merging region that spans from the merge point to the combined point (cp). At the combined point, the jets start to develop as a single jet flow in the combined region. When a wall is close enough to the nozzle exit, the jets start to deflect towards the wall and impinge on the wall at the reattachment point (rp). The region between the nozzle exit and the reattachment point is often named pre-attachment region. Downstream of the reattachment point, in the impingement region, the jet gradually develops while attached to the wall until, further downstream, the velocity profiles scale similarly to a classical wall jet (wall jet region).

2.2. Governing equations

The two-dimensional incompressible steady Reynolds-averaged equations for the transport of mass, momentum, and energy (Eq. (1)–(3)) were solved. When isothermal flow was considered (in some of the validation cases), only Eq. (1)–(2) were solved. This study is conceptual in nature and focuses on the effect of geometric parameters, specifically the offset and separation ratios, on the flow and heat transfer in confined twin jets. A two-dimensional RANS-based model was used to enable systematic parametric analysis and comparison of turbulence models at a manageable computational cost. While this approach does not resolve three-dimensional instabilities or capture spanwise effects, it provides valuable insight into the dominant two-dimensional flow features and heat transfer mechanisms relevant to engineering applications. The results should therefore be interpreted as representative of the time-averaged behavior in an idealized plane jet configuration. This simplification is common in studies of plane jets [17,23,40,42–44] and serves as a foundation for understanding more complex three-dimensional flows.

$$\frac{\partial(\rho u_j)}{\partial x_j} = 0 \tag{1}$$

$$\frac{\partial(\rho u_i u_j)}{\partial x_j} = -\frac{\partial p}{\partial x_i} + \frac{\partial}{\partial x_j}\left[\mu\left(\frac{\partial u_i}{\partial x_j} + \frac{\partial u_j}{\partial x_i} - \frac{2}{3}\delta_{ij}\frac{\partial u_k}{\partial x_k}\right)\right] + \frac{\partial(-\rho \widetilde{u'_i u'_j})}{\partial x_j} \tag{2}$$

$$\frac{\partial(\rho u_j h)}{\partial x_j} = \frac{\partial}{\partial x_j}\left[k_\mathrm{f} + \frac{c_p \mu_\mathrm{t}}{Pr_\mathrm{t}}\right]\frac{\partial T}{\partial x_j} \tag{3}$$

where x_j is the j^{th} coordinate, u_j the time-averaged velocity component in the direction j, u'_j the fluctuating velocity component in direction j, p the pressure, h the specific sensible enthalpy, T the temperature, ρ the density of air, μ the dynamic viscosity, k_f the thermal conductivity, c_p the specific heat capacity, μ_t the turbulence eddy viscosity, Pr_t the turbulent Prandtl number, and δ_{ij} the Kronecker symbol. In the present study, body forces are neglected. The properties were varied as a function of temperature. For the density, the ideal gas law was assumed and for c_p, k_f, μ the equations of Zografos et al. [45] were used.

Within the RANS approach, the Reynolds stresses (last term in Eq. (2) need to be modelled to close the equation. Since no single closure model is suitable for all flows, several turbulence models were tested in the validation section of this paper (section 3) to determine which one is more suitable for the problem addressed. As, to the best of the authors' knowledge, no experimental or numerical data exist for the flow configuration analyzed in this study, the comparison of turbulence models was performed using validation cases with common features for which experimental data is available. This approach ensures that the selected turbulence model is properly benchmarked against reliable reference data before being applied to the problem under study.

For the validation cases, the Reynolds stresses were modelled with the following widely used closure models and, as referred above, the results compared to experimental data: 1) Standard k-ε model, 2) Realizable k-ε model, 3) Standard k-ω model, and 4) Shear-stress transport (SST) k-ω model. Globally, the SST model was the one that presented a more balanced performance across all the validation cases (see section 3). Therefore, all the results presented in section 4 were obtained with the SST model. A description of the model can be found in [46,47] and the turbulence model parameters used in Table 1.

The boundary conditions used are described in Fig. 2.

At the two equal jet nozzles, uniform velocity profiles are imposed (the x-component of the velocity is calculated from *Re* and the y-component of the velocity is zero), the temperature is set to 100 °C, the turbulent intensity is 5%, and the turbulent viscosity ratio is 10. The no-slip and no-penetration boundary conditions are imposed at the solid

Table 1
Turbulence model parameters used in this study.

Model	Parameters
Standard k-ε model	$C_{1\varepsilon} = 1.44$; $C_{2\varepsilon} = 1.92$; $C_{\mu} = 0.09$; $\sigma_k = 1.0$; $\sigma_{\varepsilon} = 1.3$
Realizable k-ε model	$C_{1\varepsilon} = 1.44$; $C_2 = 1.9$; $\sigma_k = 1.0$; $\sigma_{\varepsilon} = 1.2$
Standard k-ω model	$\alpha_{\infty}^{*} = 1$; $\alpha_{\infty} = 0.52$; $\alpha_0 = 0.11111$; $\beta_{\infty}^{*} = 0.09$; $R_{\beta} = 8$; $R_k = 6$; $R_{\omega} = 2.95$; $\beta_i = 0.072$; $\sigma_k = 2.0$; $\sigma_{\omega} = 2.0$
SST k-ω model	$\alpha_{\infty}^{*} = 1$; $\alpha_{\infty} = 0.52$; $\alpha_0 = 0.11111$; $\beta_{\infty}^{*} = 0.09$; $R_{\beta} = 8$; $R_k = 6$; $R_{\omega} = 2.95$; $a_1 = 0.31$; $\beta_{i,1} = 0.075$; $\beta_{i,2} = 0.0828$; $\sigma_{k,1} = 1.176$; $\sigma_{k,2} = 1.0$; $\sigma_{\omega,1} = 2.0$; $\sigma_{\omega,2} = 1.168$

walls, which are at a constant temperature of 25 °C. A zero-diffusion flux for all flow variables was imposed at the outlet.

Since the walls were modeled with a Derichlet boundary condition (constant temperature), the local heat flux from the fluid to the horizontal walls, q_x, was computed from the temperature gradient normal to the wall using Fourier's law:

$$q_x = -k_f \frac{\partial T}{\partial y}\bigg|_{\text{wall}} \tag{4}$$

where the temperature gradient normal to the wall, $\partial T/\partial y$, was calculated using temperature values from the near-wall cells. The local Nusselt number, Nu_x, was then evaluated as:

$$Nu_x = \frac{q_x w}{k_f (T_0 - T_w)} \tag{5}$$

and the average Nusselt number along each horizontal wall was calculated by:

$$\overline{Nu} = \frac{1}{L}\int_0^L Nu_x dx \tag{6}$$

where L is the total length of the horizontal wall.

2.3. Computational domain and grid

A non-uniform structured grid was used, with a higher density of control volumes near the walls and in the jet inlet region. The grid independence study was performed for the flow configuration with $s/w = 3$ and $h/w = 4$. Three different grids were tested and the grid convergence index (GCI) was used to estimate the uncertainty due to the spatial discretization [48]. The GCI based on the area-weighted average (AWA) pressure at the top nozzle, maximum wall shear stress at the bottom wall and the maximum temperature at the outlet were computed (Table 2). The GCI values decrease as the grid is refined and the grid with 610 × 115 control volumes was considered to be a good compromise between computational time and accuracy. For this grid, the first grid point near the wall lies in the viscous sublayer ($y^+ \sim 1.0$, where y^+ is the non-dimensional wall distance to the first cell centroid).

The effect of domain size on the results was also analyzed. Different lengths of the computational domain were tested. When the lengths of the computational domain are 86 × w and 100 × w, similar results were obtained; however, smaller domain lengths lead to significant deviations in the temperature profiles obtained along the streamwise direction. Accordingly, the length of the computational domain was set to 100 × w. It was guaranteed that there were no recirculation zones at the outlet boundary for all test cases analyzed.

2.4. Numerical models and Solver

The governing equations are discretized using the finite volume method. ANSYS/Fluent v.2024 R1 [49] was used to solve the governing equations. Second-order schemes were used for all spatial discretizations, and the Semi-Implicit Method for Pressure Linked Equations (SIMPLE) was used for the pressure–velocity coupling. Convergence was achieved when the residuals of mass, velocity components, energy, turbulent kinetic energy, and specific dissipation rate were below 10^{-8}. Additionally, it was verified that the outlet temperature and the outlet turbulent viscosity ratio converged, and both the mass and energy balances were satisfied.

3. Model validation and turbulence model selection

To validate the model, three test cases were used. Since no results for a similar geometry to the one described in section 2.1 were found in the

Table 2
Grid independence study.

Control volumes	AWA static pressure @ top nozzle [Pa]	GCI [%]	Max. wall shear stress @ bottom wall [Pa]	GCI [%]	Max temperature @ outlet [Pa]	GCI [%]
382 × 58	6.87	–	0.0441	–	360.84	–
610 × 115	4.15	6.72	0.0473	2.29	360.63	0.22
1017 × 175	3.96	0.83	0.0479	0.65	360.49	0.18

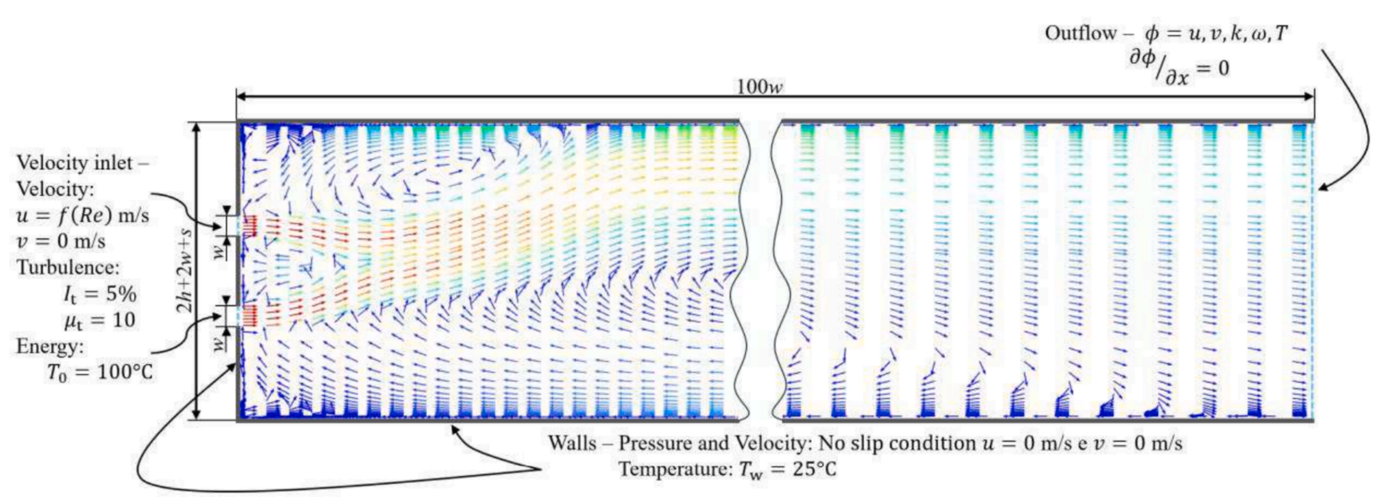

Fig. 2. Computational domain and boundary conditions used.

literature, the following configurations were used for validation: turbulent plane offset jet [9,10], heated turbulent plane offset jet [18], and twin plane turbulent isothermal free jets [6]. Combined, these configurations provide a range of flow dynamics, thermal interactions, and mixing behaviors that are foundational to the physics of confined twin plane turbulent parallel jets. The phenomena observed in these three validation cases (wall interaction, turbulence, jet deflection, entrainment, and heat transfer) are all key components of confined twin turbulent plane parallel jets.

In the first test case, described by [9,10], a plane incompressible turbulent jet is discharged from a nozzle (width $w = 12.5$ mm and depth $d = 150$ mm) into still ambient air above a wall offset by a distance h and parallel to the jet exit. The offset ratio (as defined in this paper) was set to 6.5 and the Reynolds number (based on the nozzle width and average exit velocity) to 15000.

Fig. 3 presents the comparison between several profiles of the x-component of the mean velocity along the axial direction, obtained using the present model and measured experimentally by Pelfrey and Liburdy [10]. The measurements were provided in the pre-attachment and impingement regions. Good agreement between the numerical and experimental results was obtained. The average root mean square error (RMSE) between the numerical and experimental data is 0.076, the maximum RMSE (0.11) being observed for the velocity profile at $x/w = 1$. The model is also capable of predicting the reattachment point with a deviation of 5.46%.

In the second test case, described in [18], a heated turbulent plane offset jet is discharged from a nozzle (width $w = 5$ mm and depth $d = 76.2$ mm) into still ambient air above a wall offset by a distance h and parallel to the jet exit. The Reynolds number (based on the nozzle width and average exit velocity) was set to 15000.

Fig. 4 presents the comparison between several mean non-dimensional temperature profiles along the axial direction, obtained with the present model and experimentally by Holland and Liburdy [18], for an offset ratio (as defined in this paper) of 6.5, a jet exit temperature, T_0, of 112 °C and an ambient temperature of 25 °C. The non-dimensional temperature, θ, is defined as $\theta = (T - T_\infty)/(T_0 - T_\infty)$, where T_∞ is the ambient temperature.

The average and maximum root mean square error between the numerical and experimental values are, respectively, 0.09 and 0.12, with the latter observed for the temperature profile at $x/w = 6.69$. On average, the RMSE observed in this validation case is higher than in the previous one, but still considered acceptable. The reattachment location is overestimated by 0.72%.

To introduce in the validation tests the dynamics of the interaction between two jets, a third test case was used. It consists of twin plane turbulent isothermal free jets described by Anderson and Spall [6]. In this configuration, two identical turbulent jets are discharged from a nozzle (width $w = 6.35$ mm and depth $d = 203.2$ mm) into still ambient air at constant temperature. The Reynolds number (based on a single nozzle width and average exit velocity) was set to 6000. The non-dimensional separation distance between nozzles (as defined in this paper) considered in this validation is 8.

There is a good agreement between the experimental data of Anderson and Spall [6] and the numerical results obtained with the present model for the profiles of the mean velocity along the axial direction for the combined region, but the results deteriorate in the converging region (Fig. 5). The average and maximum root mean square error observed for the velocity profiles are, respectively, 0.098 and 0.18 (the latter at $x/w = 8.81$). Anderson and Spall [6] recognize that, at this location (close to the merge point), mean flow angles approach the limit of the X-type hot-wire probe's resolution capability, which, at least partially, accounts for the discrepancy in the location of the velocity peak between experiments and numerical results. Additionally, the experimental results show no decay to zero of the mean velocity outside the jet envelope due to transverse entrainment and measurement limitations in low-velocity ranges [6].

All the above results were obtained with the SST k-ω model for turbulence closure. This was the model that, overall, showed the best agreement with the experimental data across the three validation cases. In Table 3, the performance of four widely used turbulence models in predicting flow reattachment in offset jets is compared.

The two turbulence models that best predict the recirculation length for the offset jets are the standard k-ε with enhanced wall treatment (EWT) and the SST model. For the Pelfrey and Liburdy configuration [9,10], the k-ε EWT performs better (0.08% absolute relative error), but in the case of Holland and Liburdy [18], the most accurate model is the SST (0.72% absolute relative error). In the prediction of the combined point location of the twin free jets, the model with the lowest absolute relative error is the standard k-ω (4.80%), followed by the k-ε EWT model (7.95%). For both the reattachment and combined points, the

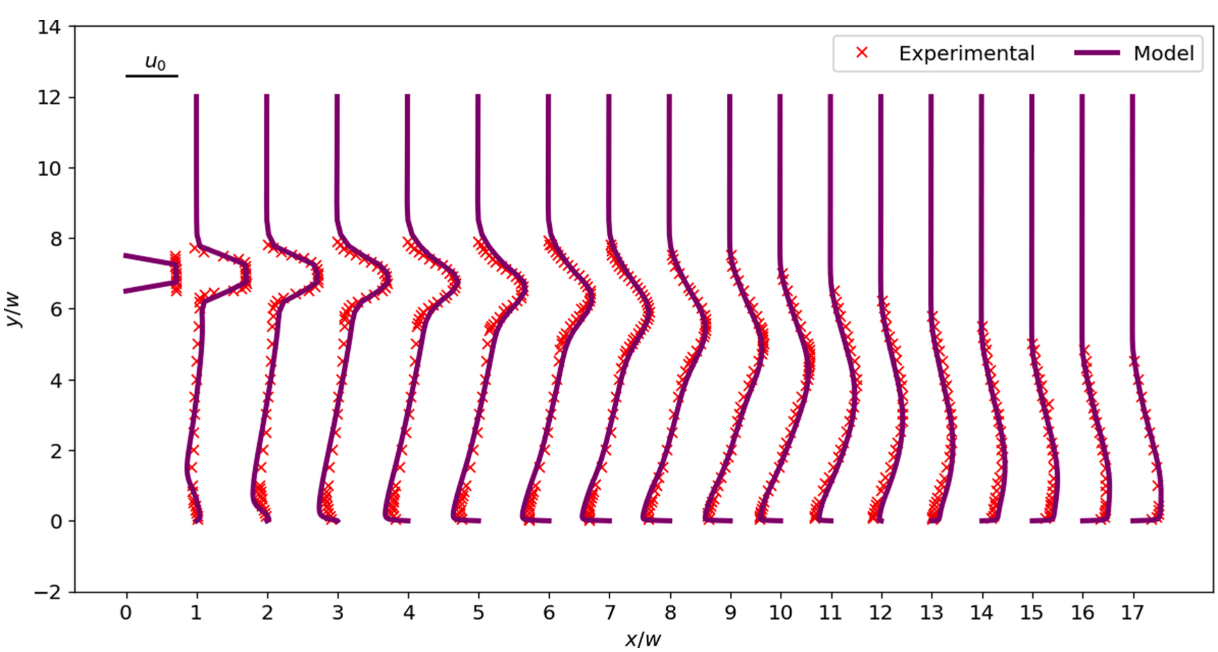

Fig. 3. Model validation with the experimental results of Pelfrey and Liburdy [10] for a turbulent plane offset jet.

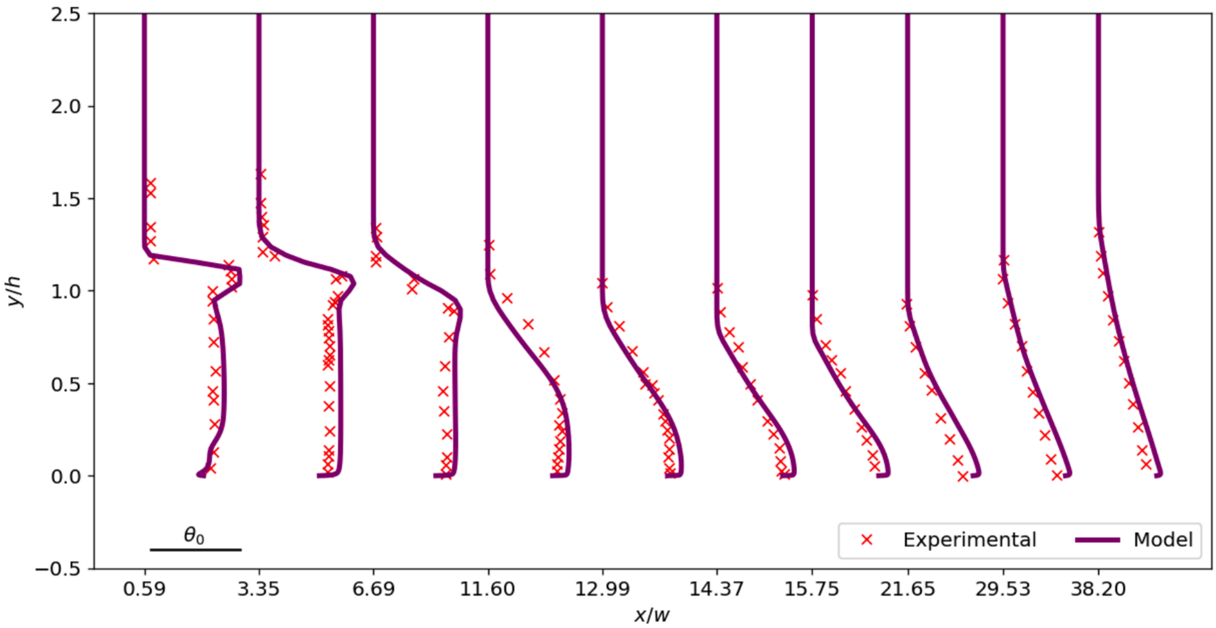

Fig. 4. Model validation with the experimental results of Holland and Liburdy [18] for a heated turbulent plane offset jet ($h/w = 6.5$, $T_0 = 112$ °C).

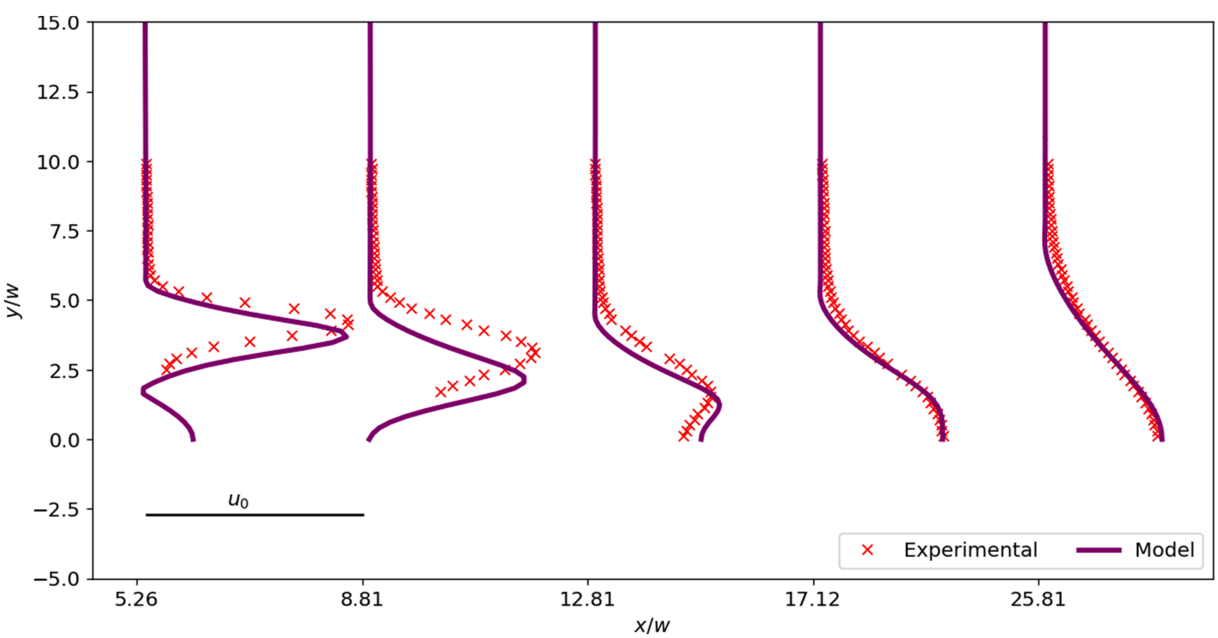

Fig. 5. Model validation with the experimental and numerical results of Anderson and Spall [6] for twin plane turbulent isothermal free jets ($s/w = 8$; only one jet is shown, since the flow is symmetrical).

model that performs the worst is the realizable k-ε with enhanced wall treatment (Real. k-ε EWT). However, this is the model that better predicts the merge point, with a deviation from the experimental value of Anderson and Spall [6] of 11.73%, while the k-ε EWT (24.22%) and the SST model (25.33%) show a much worse performance. However, Anderson and Spall [6] point out that it was difficult to determine the merge point experimentally by hot-wire anemometry due to the sensor's lack of reverse flow sensitivity, so this parameter was obtained from the measured streamwise Reynolds normal stress. All the models underestimate the merge and the combined points. This underestimation was also observed by Hnaien et al. [50] ($x_{mp}/w = 9.49$ and $x_{mp}/w = 17.61$).

The mean velocity along the symmetry plane for the twin plane turbulent isothermal free jets studied by Anderson and Spall [6] is presented in Fig. 6 (The velocities are non-dimensionalized by the jet exit velocity, u_0). In the converging and merging regions, the model that better approximates the experimental results is the realizable k-ε with enhanced wall treatment. However, in the combined region, the SST and the k-ε EWT models perform better, with both showing similar results. Globally, these two models present a RMSE of 0.05 (SST) and 0.04 (k-ε EWT).

The maximum velocity, $|\mathbf{v}|_{max}$, decay along the axial direction for the turbulent plane offset jet studied by Pelfrey and Liburdy [10] is better predicted by the k-ε EWT model (Fig. 7), while the SST model is the most accurate for the prediction of the scaled wall shear stress, τ_w, where τ_{max} is the maximum wall shear stress downstream of impingement (Fig. 8). Globally, these two models present a RMSE of 0.05 (SST) and 0.03 (k-ε EWT) for the maximum velocity decay and 0.06 (SST) and 0.20 (k-ε EWT) for the wall shear stress.

Table 3
Non-dimensional impingement location for the offset jets studied by Liburdy and co-workers [9,10,18] and non-dimensional merge and combined points location for the twin jet studied by Anderson and Spall [6].

	Experiments	k-ε EWT	Real. k-ε EWT	k-ω	SST
Pelfrey and Liburdy [10]					
x_{rp}/w	13.0	12.99	10.32	10.63	12.29
RE (%)	–	0.08	20.62	18.23	5.46
Holland and Liburdy [18] ($h/w = 6.5$, $T_0 = 112$ °C)					
x_{rp}/w	12.42	13.08	10.14	13.21	12.33
RE (%)	–	5.31	18.36	6.36	0.72
Anderson and Spall [6] ($s/w = 8$)					
x_{mp}/w	11.85	8.98	10.46	8.27	8.73
RE (%)	–	24.22	11.73	30.21	25.33
x_{cp}/w	19.36	17.82	17.00	18.43	17.61
RE (%)	–	7.95	12.19	4.80	9.04

For the heated turbulent offset jet studied by Holland and Liburdy [18], in the pre-attachment region nearer the nozzle plane, the realizable k-ε is the model that best approaches the experimental results, closely followed by the other models (Fig. 9). None of the models is very good at predicting the decay of the maximum jet temperature in the vicinity of the impingement point. Globally, the realizable k-ε model presents an RMSE of 0.07 and the other models 0.08.

Other comparative studies of the performance of various turbulence models used on CFD studies of similar turbulent jets have been presented in the literature. Nasr and Lai [41] compared three turbulence models (standard k-ε [51], Renormalization Groups (RNG) k-ε [52], and Reynolds-stress [53] models) for predicting a turbulent plane offset jet with a small offset ratio, concluding that while the models quantitatively capture the key flow regions, the standard k-ε model provides the most accurate predictions of the reattachment length. Rathore and Das [16] showed that, while both the standard k-ε model and the low-Reynolds number turbulence model by Launder and Sharma [54] predict the turbulence behavior of offset jets, the low-Reynolds model by Yang and Shih [55] performs better, especially in accurately resolving near-wall fields, skin friction, and capturing Moffatt vortices, with closer agreement to experimental results from various studies. Later on, Rathore and Das [56] compared the same turbulence models and additionally the Shear Stress Transport (SST) [57] model for heat transfer in offset and wall jets. They conclude that the SST model provides the most accurate results across a range of conditions. This was also the model chosen by Ajmi et al. [23], who compared its performance to three other turbulence model (RNG k-ε, realizable k-ε, standard k-ω). The study of Hnaien et al. [33] compares five turbulence models to assess their accuracy in predicting wall and offset jets. The models considered were the standard k-ε, RNG k-ε, realizable k-ε, standard k-ω, and SST models [49]. These authors concluded that the standard k-ω provides the most reliable predictions and the realizable k-ε performs the worst. Assoudi et al. [42], in a comparison between the standard k-ε model and the Reynolds Stress Model, shows that the RSM provides superior accuracy. The same conclusion was made by Anderson and Spall [6], when comparing the standard k-ε model and the RSM for the simulation of twin free parallel jets. Hnaien et al. [50] reached a different conclusion. These authors compared the performance of three turbulence models (standard k-ε, standard k-ω and RSM) for the prediction of the twin jets configuration of Anderson and Spall [6] and concluded that the standard k-ε model presents the best results. On another study, Li et al. [58] present a comparison of two turbulent models for twin parallel jets. In this study the realizable k–ε and the SST produced comparable results, with the realizable k–ε performing slightly better.

Based on the validation of the three test cases presented in this section, the k-ε with enhanced wall treatment (k–ε EWT) and the shear stress transport k-ω (SST) turbulence models consistently demonstrated the most accurate performance. The k–ε EWT performed better in cases without heat transfer, particularly in the prediction of the recirculation length and velocity decay in offset jets. However, the SST model showed a more balanced performance across all three validation cases. It proved more effective in capturing thermal interactions and offers a balanced performance in the twin jet configuration. Given the importance of modelling wall interactions, jet deflection and heat transfer in the present study, the SST model was selected as the more robust and versatile choice.

4. Results and discussion

4.1. Flow characteristics

Fig. 10a and 10b show the time-averaged streamlines and velocity

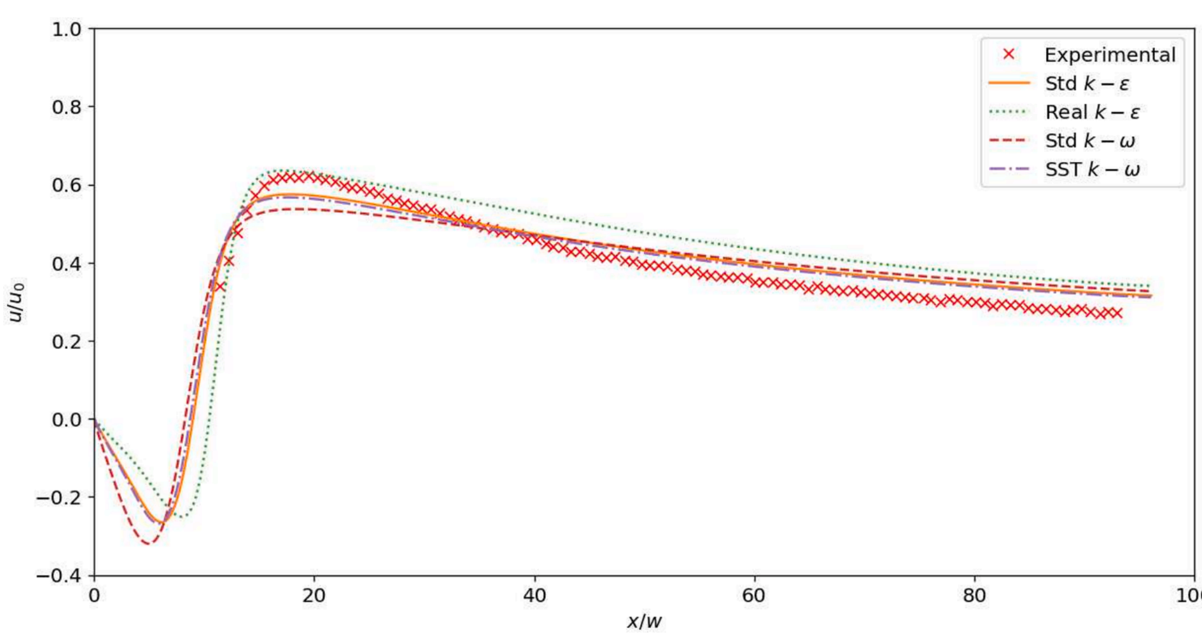

Fig. 6. Numerical and experimental mean non-dimensional velocity along the symmetry plane for the twin plane turbulent isothermal free jets studied by Anderson and Spall [6] ($s/w = 8$).

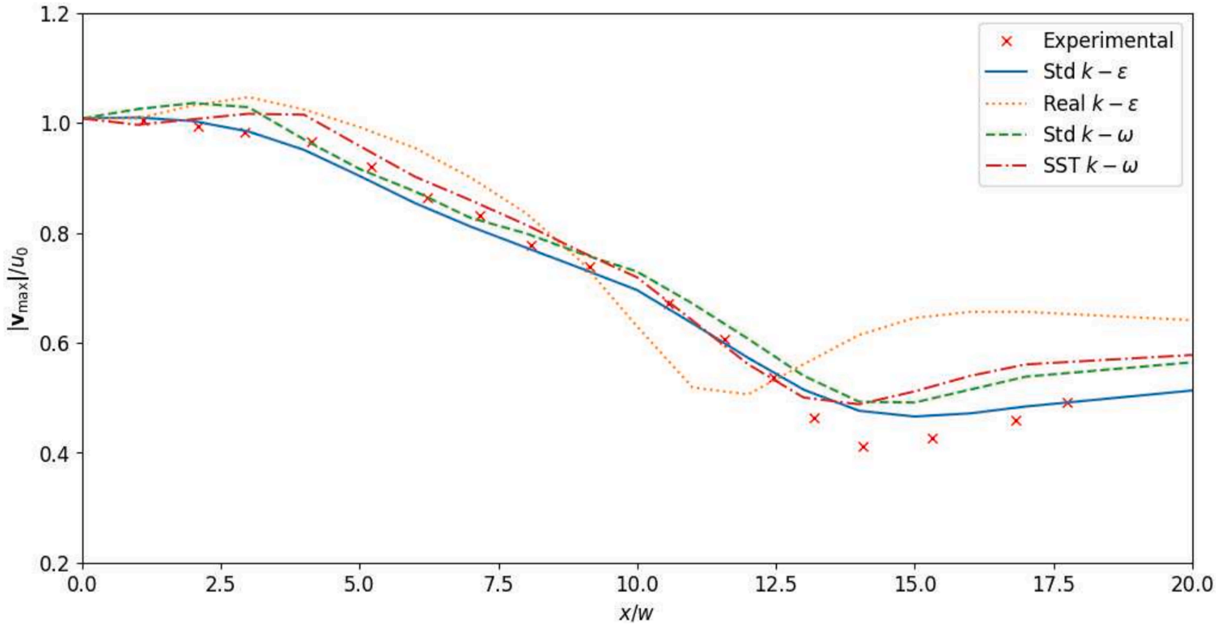

Fig. 7. Numerical and experimental non-dimensional maximum velocity decay along the axial direction for the turbulent offset jet studied by Pelfrey and Liburdy [10].

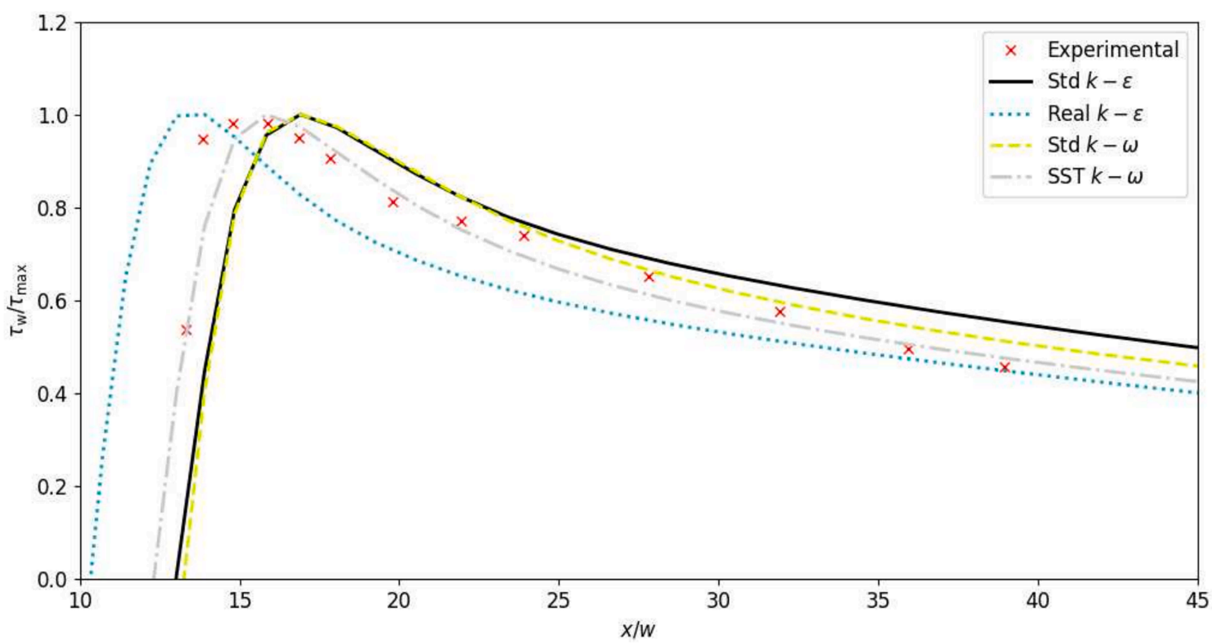

Fig. 8. Numerical and experimental non-dimensional x-component of the shear stress along the wall for the turbulent offset jet studied by Pelfrey and Liburdy [10].

vectors, respectively, both colored by the velocity magnitude, while Fig. 10c presents the time-averaged streamlines colored by static pressure. These figures correspond to a separation ratio, s/w, of 3 and an offset ratio, h/w, of 4. The color scheme ranges from blue (lower values) to red (higher values). These three figures provide insight into the interaction between pressure and velocity fields, which helps in understanding the flow field behavior. As shown, once the two jets enter the domain, they begin to deflect towards each other due to the low-pressure zone that forms between them, caused by the mutual entrainment of the air. In this region, two low-pressure, counter-rotating vortices form between the two jets, further intensifying the low-pressure area. At a certain distance from the nozzles, x_{mp}, the inner shear layers of the two jets come into contact at the merge point, which is located between a region of low velocity and low pressure, and another of low velocity and relatively high pressure. For this flow configuration, the merge point, where the velocity is zero, is located at $(x/w, y/w)_{mp} = (4.05, 0.26)$. Note that the merge point lies slightly above the centerline between the two horizontal walls, and the two counter-rotating vortices are asymmetrical with respect to this centerline, unlike in the case of free twin plane jets, where symmetry would typically be observed [6]. The merge point location obtained for this configuration is comparable to the results of Nasr and Lai [5] for two free parallel jets with a separation ratio of 3.25, $(x/w, y/w)_{mp} = (4, 0)$, and larger than the results of Fujisawa et al. [7] for a separation ratio of 3, $(x/w, y/w)_{mp} = (3, 0)$. These two studies focused on free plane parallel jets, being the flow symmetric. Flow asymmetry is present in the configuration analyzed by

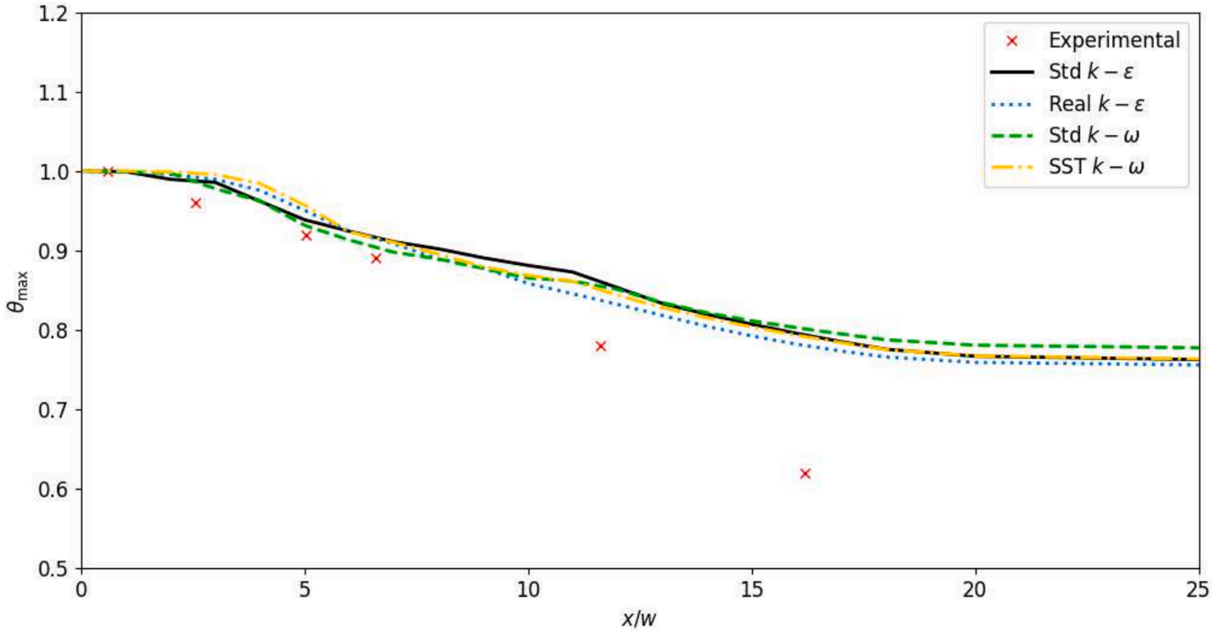

Fig. 9. Numerical and experimental maximum non-dimensional temperature along the axial direction for the heated turbulent offset jet studied by Holland and Liburdy [18].

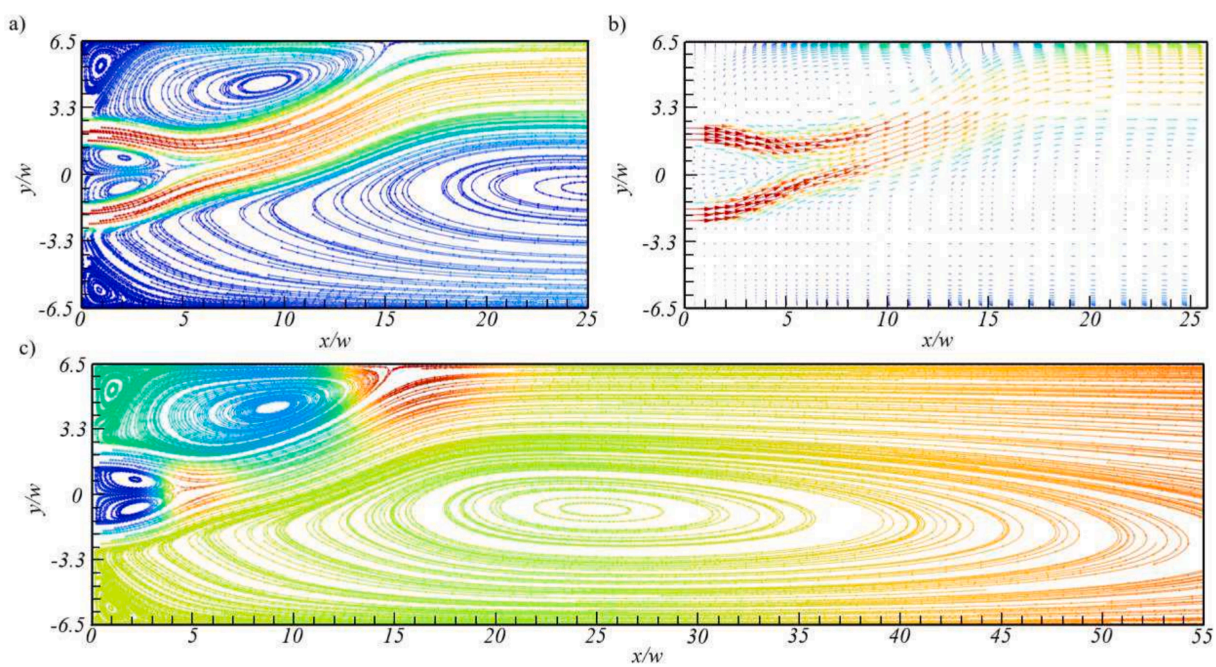

Fig. 10. a) Streamlines and b) velocity vectors colored by velocity magnitude, and c) streamlines colored by static pressure for two confined turbulent plane parallel jets with $s/w = 3$, $h/w = 4$ and $Re = 15000$.

Mondal and Pramanik [39], who studied a configuration similar to the one studied in this paper but with only one wall at the bottom and no heat transfer. In Mondal and Pramanik [39], $(x/w,\ y/w)_{mp} = (3.78, -0.28)$ for a separation ratio of 3 and an offset ratio of 2.5. (For interpretation of the references to color in this figure legend, the reader is referred to the web version of this article.)

Fig. 10 also shows that, after the merge point, the (not-yet-fully) combined jet deflects toward the top wall due to the Coandă effect. This deflection is driven by the low pressure in the region between the jet and the top wall, which results from the entrainment of air. An imbalance in entrainment between the two sides of the jet reinforces the pressure asymmetry, which feeds the deflection process and creates a feedback loop that sustains the deflection, helping the jet to stay attached to the surface.

The flow asymmetry described above arises despite the configuration being symmetric in relation to the x-z plane located at $y = h + w + s/2$. In some cases (like the one depicted in Fig. 10), the jet deflects upwards, while in others, it deflects downwards, and then impinges on the top or bottom wall, respectively. The asymmetry and variable direction of deflection (sometimes upwards other times downwards) were also observed experimentally, for example, by Salvador et al. [1]. This behavior is influenced by both the Coandă effect and instabilities in the flow. Even though the setup is symmetrical, a jet is inherently unstable, especially when it is in close proximity to a wall. Turbulence can amplify small disturbances and cause the jet to deflect to one side, which in turn triggers the Coandă effect. Once deflected, the Coandă effect causes the jet to adhere to the top or bottom wall, leading to steady flow behavior. The attachment of the jet to the wall stabilizes the flow and the jet behaves similarly to an offset jet, staying attached to one wall despite the initial symmetry. Small asymmetries, such as slight misalignment of the nozzle or uneven inlet velocity distribution, can also contribute to the initial deflection. Even in idealized simulations such as the one performed in this study, several factors (e.g., round off-errors or the way the equations are solved) contribute to the flow asymmetry, mimicking real-world effects.

The flow deflection towards the wall and subsequent attachment results in the formation of a vortex between the impingement wall, the nozzle plate and the jet. For the conditions reported in Fig. 10, the length of this recirculation is $x_{rp}/w = 15.09$ (the recirculation point is calculated as the location where the x-component of the velocity changes sign). This point is located downstream of the reattachment point reported by Mondal and Pramanik [39] for a configuration similar to the one studied in this paper but with only one bounding wall and no heat transfer and an offset ratio of 2.5 ($x_{rp}/w = 10.85$). As will be seen later, the reattachment point moves upstream with the reduction of the offset ratio and, consequently, approaches the value given by Mondal and Pramanik [39]. Fig. 10 also shows that at the corner where the vertical and horizontal walls meet, secondary vortex flows are present.

Due to the confinement of the flow between the two horizontal walls, a large clockwise vortex forms between the bottom wall and the jet (Fig. 10). This recirculation zone extends from the converging region to the combined region and is primarily shaped by the interaction between the jet flow and the bottom wall.

Fig. 11 shows profiles of the mean x-component of the velocity vector at several downstream locations. The first velocity profiles ($x/w = 0.54$, 2.58, and 3.6) show the two counter-rotating vortices that form in the region between the two jets (negative mean x-component of the velocity). At $x/w = 5.13$, the two jets have already merged and no recirculation between them exists; however, the velocity profile still exhibits two peaks, since the jets are still not entirely combined to form a single jet flow. The combined point, the location where the velocity profile assumes a form with only one peak, is located at $(x/w, y/w)_{cp} = (12.53, 2.29)$ for this flow configuration. After this point, the velocity profile exhibits only one peak. The recirculation zones at the bottom and top walls are also clearly visible in Fig. 11. At $x/w = 15.34$ the flow is completely reattached to the top wall, but it is not until $x/w = 86$ that Fig. 11 shows no reverse flow at the bottom wall.

The combined point obtained in this case ($s/w = 3$, $h/w = 4$) is located downstream and closer to the wall than the combined point reported by Mondal and Pramanik [39], who studied a configuration similar to the one studied in this paper but with only one bounding wall and no heat transfer. In Mondal and Pramanik [39] $(x/w, y/w)_{mp} = (11.74, -1.24)$ for a separation ratio of 3 and an offset ratio of 2.5.

The evolution of the maximum mean jet velocity along the axial direction is shown in Fig. 12 for $h/w = 4$ and various s/w and in Fig. 13 for $s/w = 3$ and several h/w. Downstream of a very short potential core region, the maximum jet velocity experiences a slight increase due to the low-pressure region near the nozzle plate. After this initial acceleration, the maximum velocity drops sharply as the flow approaches the reattachment point. At this point, the airflow separates and becomes predominantly tangential to the horizontal wall: part of the flow moves away from the nozzle plate, while the rest moves in the opposite direction. After a local velocity minimum slightly upstream of the reattachment point, the portion of the fluid flowing downstream accelerates due to a favorable pressure gradient. As a result, it reaches a local velocity maximum, and afterwards, the maximum mean jet velocity decays at a lower rate than in the pre-attachment region and approaches a value of around 25% of the jet exit velocity at $x/w = 100$. Also noticeable are slight bumps in the velocity decay downstream of the merge point and upstream of the reattachment point. Instead of a smooth and rapid decay in peak velocity, the rate of velocity decay slows locally, or the velocity even increases, depending on the values of the geometrical parameters.

The separation ratio of the two jets was varied between 2 and 5, with the offset ratio kept constant at 4, to analyze the influence of this parameter on the flow behavior. It can be observed that as the separation distance increases (with the offset distance held constant), the local minimum velocity near the reattachment point decreases and the point itself shifts downstream. The latter is also shown in Fig. 14, which depicts the non-dimensional locations of the points of interest. The different colors represent different geometrical parameters, while the

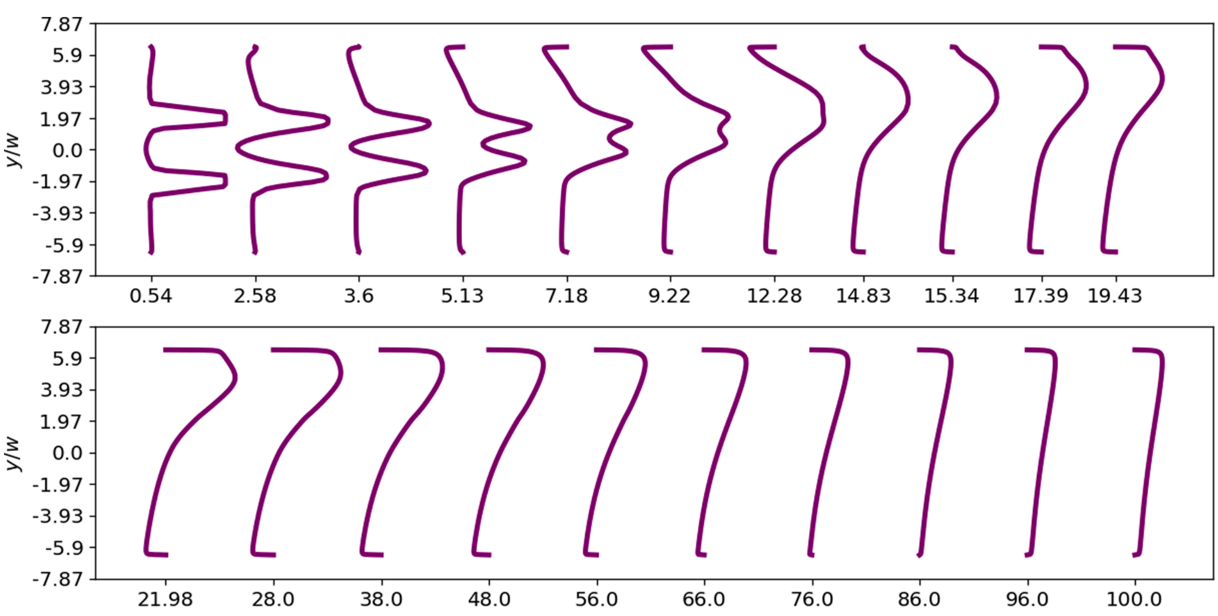

Fig. 11. Profiles of mean x-component of the velocity at several non-dimensional locations, x/w, for two confined turbulent plane parallel jets with $s/w = 3$, $h/w = 4$ and $Re = 15000$.

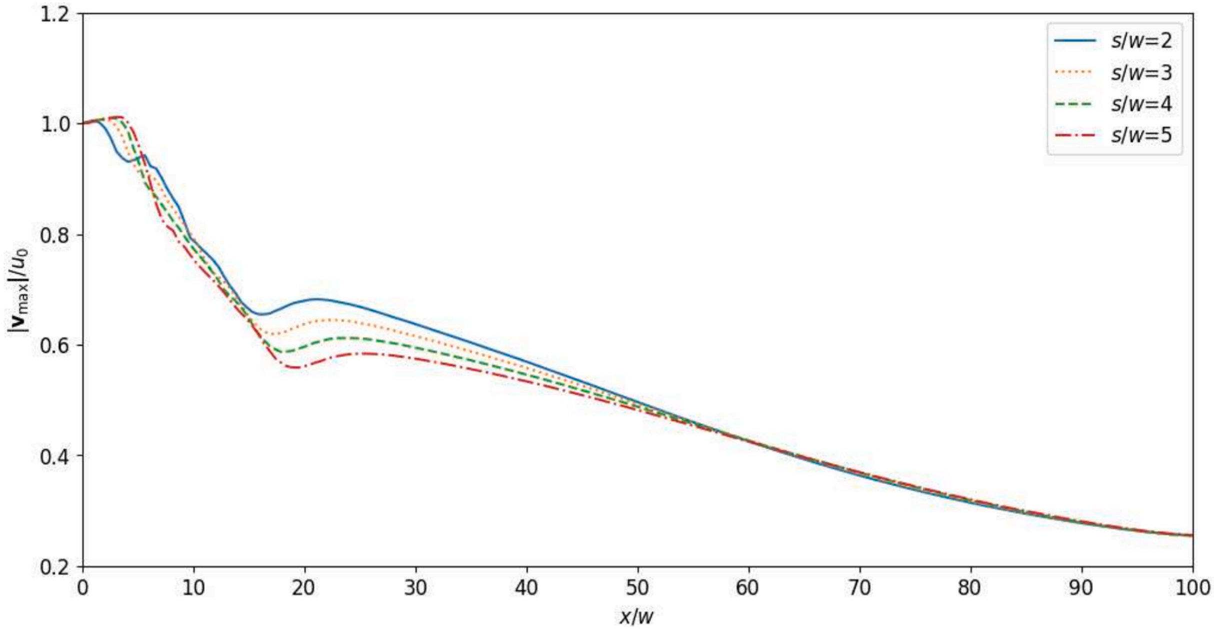

Fig. 12. Maximum mean velocity decay of the two confined turbulent plane parallel jets with $h/w = 4$, $Re = 15000$ and several separation ratios.

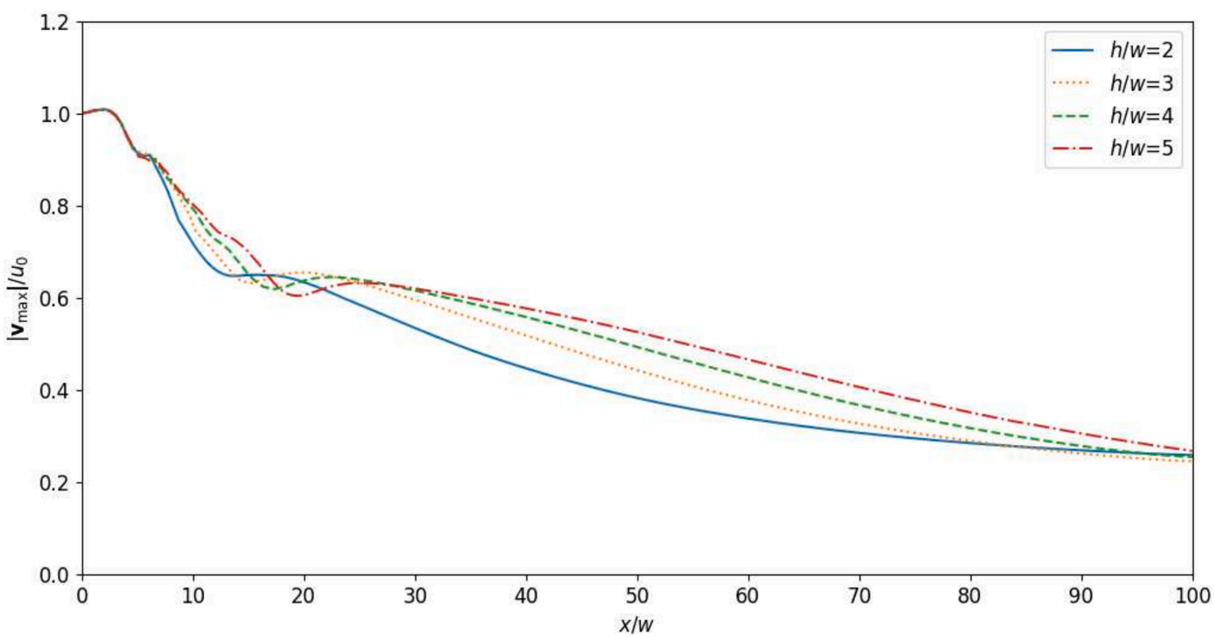

Fig. 13. Maximum mean velocity decay of the two confined turbulent plane parallel jets with $s/w = 3$, $Re = 15000$ and several offset ratios.

symbols denote the points of interest: a circle for the recirculation point, a left-pointing triangle for the merge point and a right-pointing triangle for the combined point. The vertical axis was plotted as $|y|/w$ and not y/w to show more clearly that the direction of deflection does not alter the underlying trends and that the lengths of the converging, merging and pre-attachment regions depend on $|y|/w$, not its sign.

For a fixed offset ratio, as the jet separation ratio increases, so does the length of the two counter-rotating vortices between the two jets near the nozzle plate and, consequently, the position of the merge point and combined point generally shifts downstream. The increase of the merging length with the increase in the separation distance between the two nozzles is due to a weaker interaction between jets. Downstream of the merge point, the jet gains some momentum. This is more visible for the lowest separation ratio ($s/w = 2$), where the jet locally accelerates. For the other separation distances, there is no local increase in velocity, but the rate of velocity decay slows down (Fig. 12).

After varying the separation ratio, this parameter was kept constant ($s/w = 3$) and the offset ratio was varied between 2 and 5. Figs. 13 and 15 show that, for a fixed separation ratio, as the offset ratio increases, the reattachment length increases and the local minimum of $\mathbf{v}_{max}$ decreases. The effect of the offset ratio on the location of the merge and combined points is not always so straightforward. The length of the combined region increases when h/w is varied from 2 to 4 but remains practically constant for $h/w = 5$. On the other hand, the location of the merge point is not very sensitive to the offset ratio. A larger offset distance lengthens the merging region and delays wall impact with the consequent weakening of the intensity of wall impingement. With more space to evolve before interacting with the wall, the jet spreads out

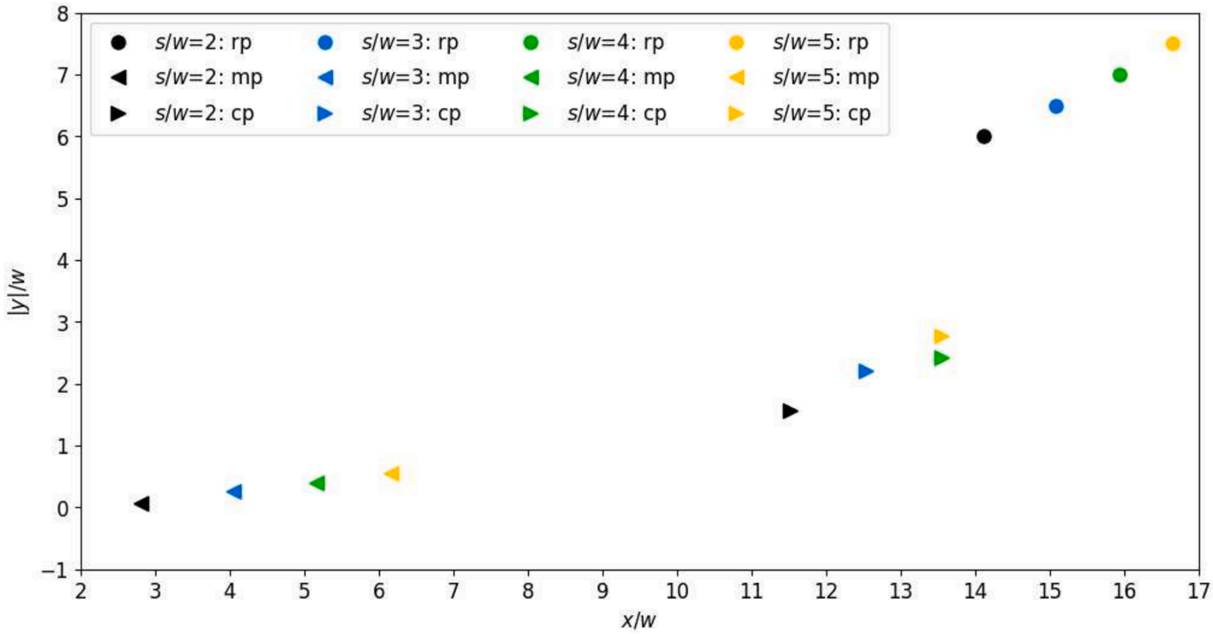

Fig. 14. Points of interest for two confined turbulent plane parallel jets with $h/w = 4$, $Re = 15000$ and several separation ratios.

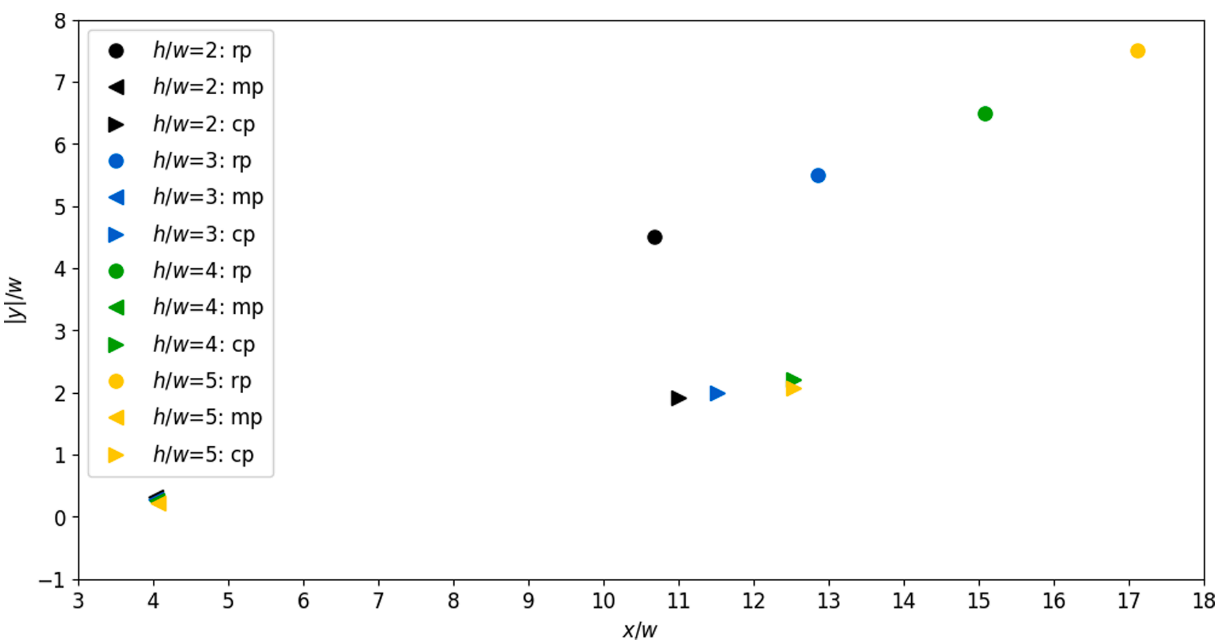

Fig. 15. Points of interest for two confined turbulent plane parallel jets with $s/w = 3$, $Re = 15000$ and several offset ratios.

more, which reduces the velocity near the reattachment point.

An interesting observation is that the jet deflects downwards in some cases and upwards in others. The cases where the jet impinges on the bottom wall are: $h/w = 4$ with $s/w = 2$, and $s/w = 3$ with $h/w = 2$. In all other cases, the jet deflects towards the upper wall. This observation supports the earlier discussion of the asymmetric behavior of the twin plane parallel jets in a symmetrical configuration. Note that, due to the varying separation or offset distances, the walls are not positioned at the same $|y|/w$.

The absolute value of the wall shear stress along the wall towards which the jets deflect (the impingement wall) generally increases until reaching a maximum, after which it decreases (Figs. 16 and 17). In the pre-attachment region, the wall shear stress is negative because of the flow reversal caused by an adverse pressure gradient. After reattachment, the shear stress becomes positive as the boundary layer redevelops in the direction of the main flow. As the flow accelerates, the wall shear stress increases to a peak. Further downstream, the jet behaves like a wall jet flow for all separation and offset ratios.

On the opposite wall, the absolute value of the wall shear stress remains relatively small and stable compared to the impingement wall. Here, the shear stress is negative over a long region due to the recirculation flow, but it eventually becomes positive. The strength of this recirculation, and its impact on the surface, is relatively insensitive to changes in separation ratio (for a fixed offset ratio), whereas varying the offset ratio leads to more significant differences.

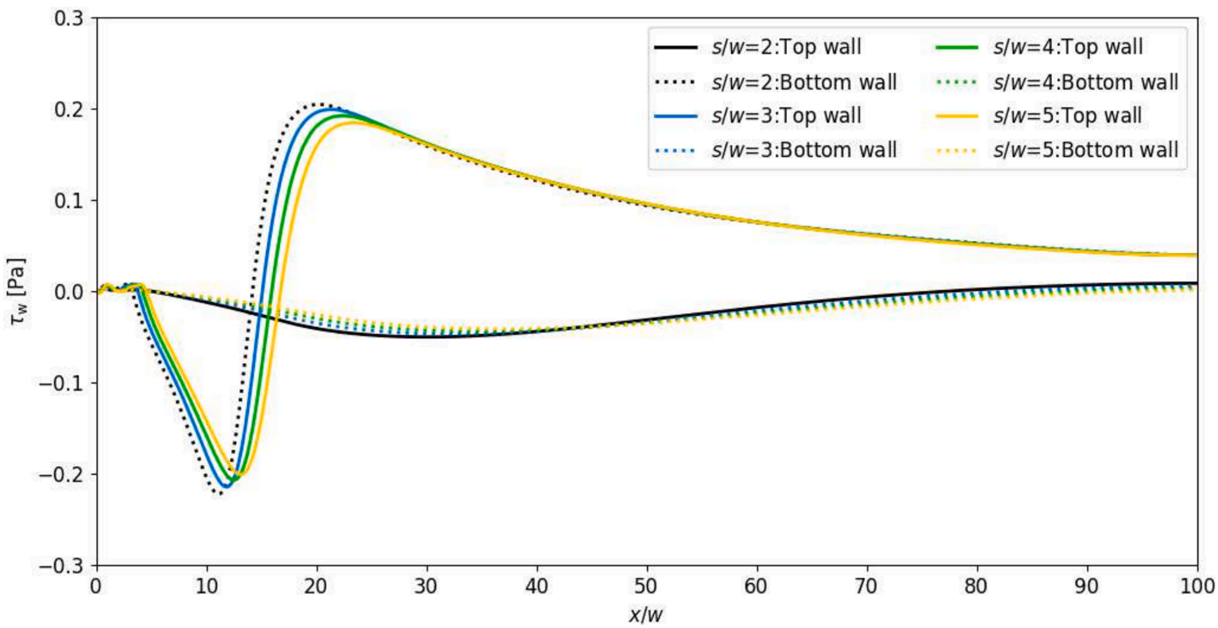

Fig. 16. Wall shear stress along the top and bottom walls for two confined turbulent plane parallel jets with $h/w = 4$, $Re = 15000$ and several separation ratios.

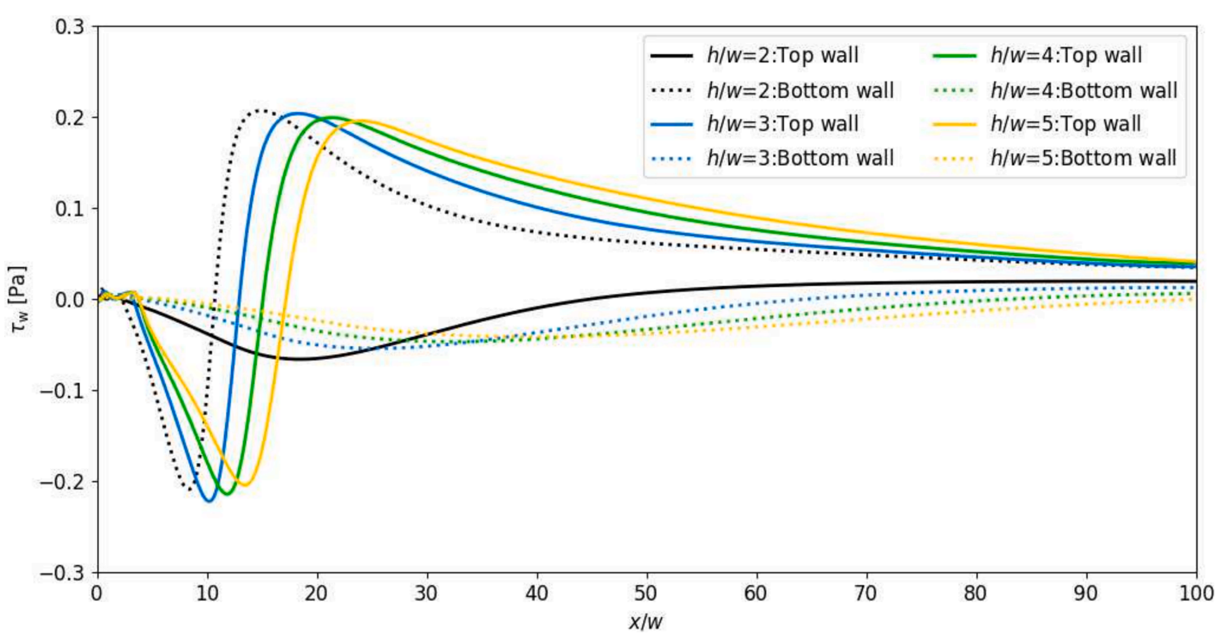

Fig. 17. Wall shear stress along the top and bottom walls for two confined turbulent plane parallel jets with $s/w = 3$, $Re = 15000$ and several offset ratios.

4.2. Heat transfer

Heat transfer plays a fundamental role in the behavior of confined jets, influencing energy distribution and thermal boundary layer development. Unlike air free jets at relatively low temperatures, where heat transfer is primarily driven by turbulent mixing with the ambient fluid, confined jets are influenced by additional factors such as wall interactions, including recirculation zones and thermal boundary layer constraints, which can significantly alter heat distribution and flow behavior.

Fig. 18 shows streamlines colored by mean temperature for the confined dual jet with separation and offset ratios of 3 and 4, respectively. As shown, the jets are responsible for bringing thermal energy into the domain, while the colder walls impose large temperature gradients in specific regions of the flow field. The converging region between the two jets is only minimally affected by the wall temperature due to constant mixing in the vortices that form between the jets. On the top wall, the recirculation zone created by the upper shear layer of the deflected jet shows a lower temperature than the jet exit temperature, with the temperature rising slowly in the downstream direction to reach a maximum when in contact with the jet shear layer in the vicinity of the reattachment point. Additionally, the influence of the wall temperature is clearly visible in the region of intersection of the vertical and horizontal walls, where the corner vortices exhibit lower temperatures.

Temperature profiles along several downstream locations are shown in Fig. 19. These profiles confirm the previously described behavior. Near the nozzle plate, at $x/w = 0.54$, the largest temperatures occur at the core of the two distinct jets, decreasing sharply in the outer shear

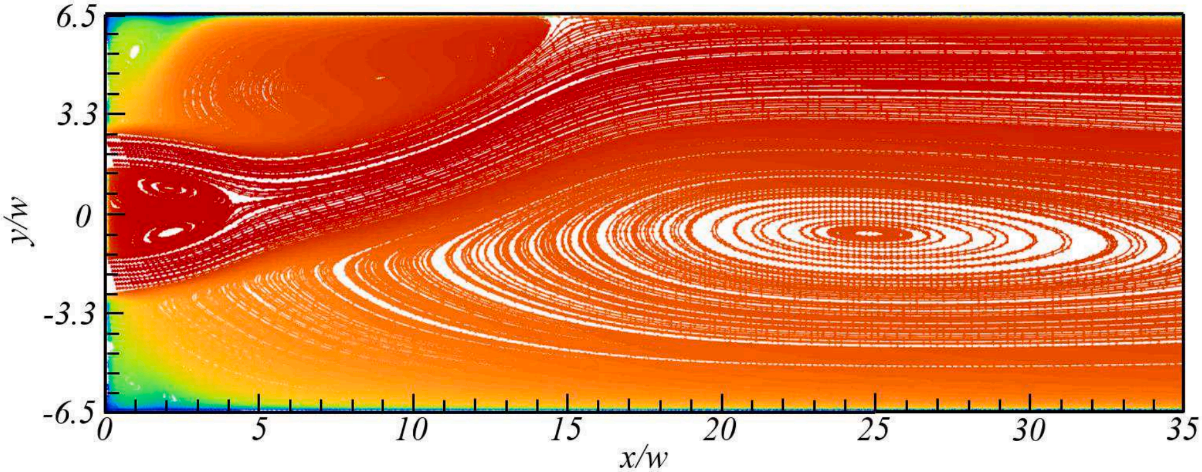

Fig. 18. Streamlines colored by temperature for two confined turbulent plane parallel jets with $s/w = 3$, $h/w = 4$ and $Re = 15000$.

layers of the two jets. Between the two jets, the temperature is slightly lower than the jet exit temperature, due to the influence of the wall at a lower temperature, but high due to the intense mixing imposed by the two counter-rotating vortices. As the flow progresses downstream, the temperature in the region of the two counter-rotating vortices approaches the maximum temperatures of the two jets. Also, the temperature of the large vortices near the bottom and upper walls slowly increases, showing a fairly constant value along y/w, except near the walls where there is a sharp temperature gradient. The temperature gradient at the wall is higher for the upper vortex than the bottom vortex. Contrary to what happens with the velocity profiles, before the combined point, $x/w_{cp} = 12.53$, the temperature profiles already show only one maximum. This maximum weakens and moves closer to the upper wall as the combined jet flows downstream.

Figs. 20 and 21 show the decay of the maximum non-dimensional temperature, θ_{max}, along the axial direction, where $\theta = (T - T_w)/(T_w - T_0)$; where T_w is the wall temperature, and T_0 is the temperature of the jets at the nozzle exit. After an initial length where the maximum mean temperature remains equal to the jet temperature, the maximum temperature begins to decay. Fig. 20 shows that, for a fixed offset ratio, increasing the separation ratio causes the temperature to decay more rapidly at first. However, the curves converge at around $x/w \approx 80$. Beyond this point, the non-dimensional temperature is slightly higher for the highest separation ratios. The effect of increasing the offset ratio (Fig. 21) is less straightforward than that of the separation ratio. As the jets deflect towards the wall, the temperature decay shows little sensitivity to the offset ratio. Downstream impingement, the jet with the largest offset ratio reaches the lowest θ_{max} values, while the jet with the smallest offset ratio has the highest θ_{max} values. After $x/w \sim 80$, the values of θ_{max} for all four offset ratios become very similar, although the lowest offset ratio consistently exhibits the highest θ_{max} values.

Figs. 22 and 23 show the local Nusselt number, Nu_x, along the bottom and top walls for several separation and offset ratios. Generally, the local Nusselt number at the wall where the jet impinges increases sharply from the nozzle plate to the reattachment point, and then decreases more gradually along the wall. This behavior has been reported by several authors for offset jets [19,23]. On the wall opposite to the jet

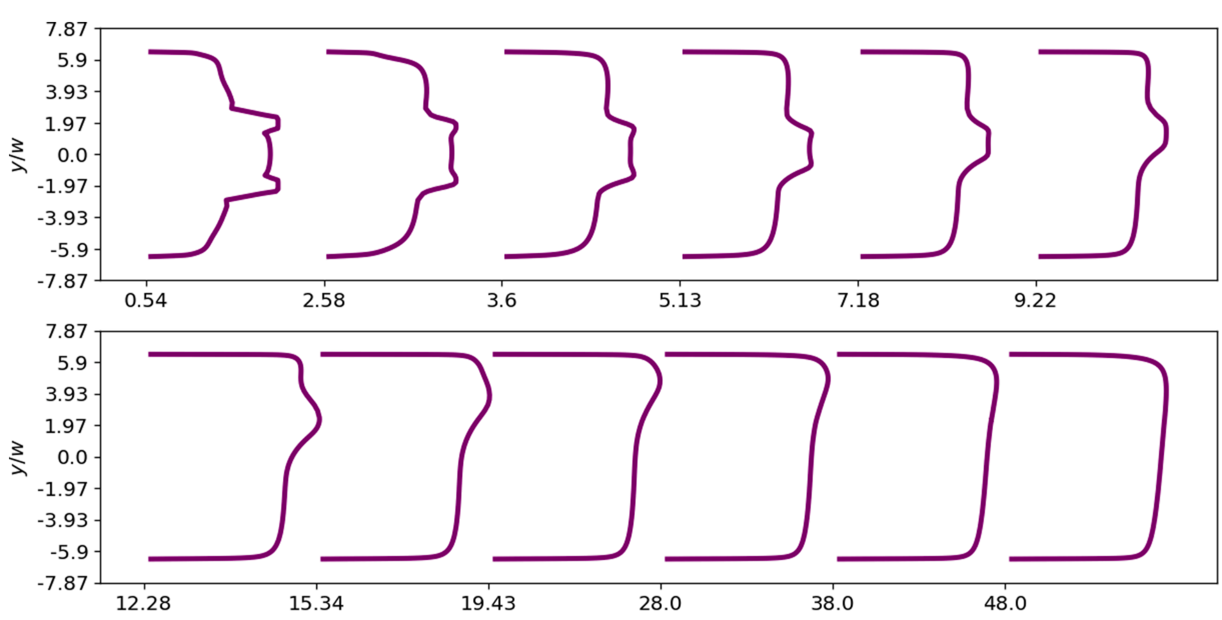

Fig. 19. Profiles of mean temperature at several non-dimensional locations, x/w, for two confined turbulent plane parallel jets with $s/w = 3$, $h/w = 4$ and $Re = 15000$.

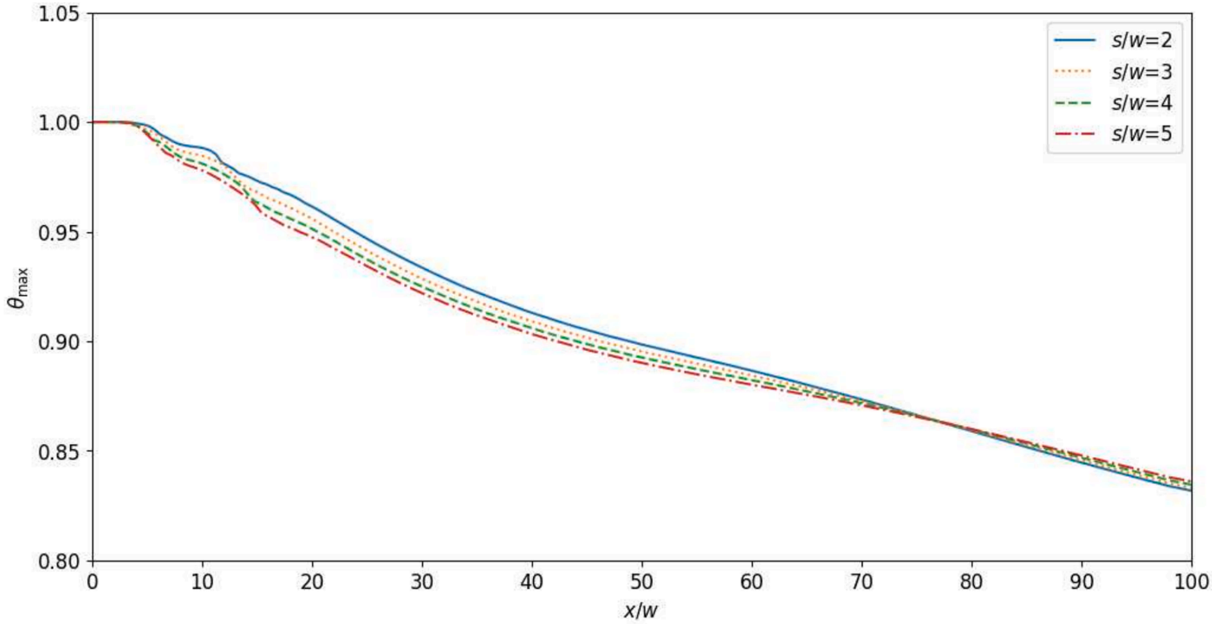

Fig. 20. Maximum mean non-dimensional temperature decay of two confined turbulent plane parallel jets with $h/w = 4$, $Re = 15000$ and several separation ratios.

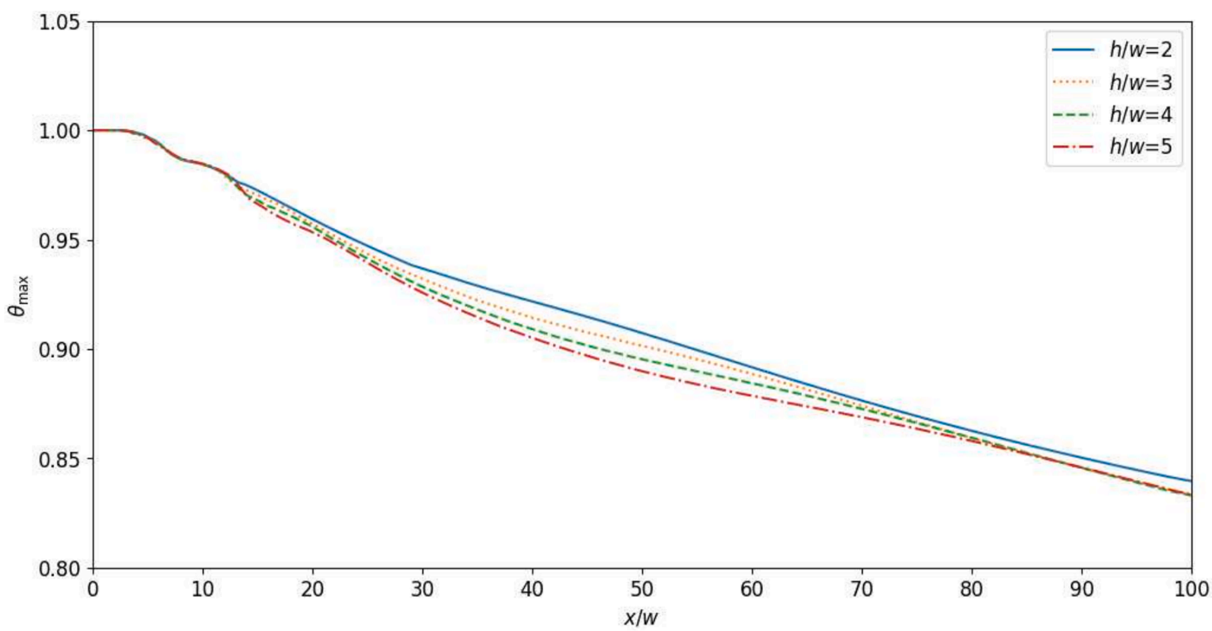

Fig. 21. Maximum mean non-dimensional temperature decay of two confined turbulent plane parallel jets with $s/w = 3$, $Re = 15000$ and several offset ratios.

impingement, the maximum local Nusselt number is significantly lower than that of the impingement wall and its rate of increase is also slower. Additionally, near the corners where the horizontal and vertical walls meet, other much smaller Nu_x peaks are observed. These maxima correspond to the locations of small secondary vortices that form at the corners.

For a fixed offset ratio of 4, as the separation ratio increases, the peak Nusselt number on the impingement wall moves downstream, similar to the reattachment point (see Fig. 14). As the wall jet develops, the local Nusselt number approaches a value that becomes independent of the separation distance. The effect of the separation ratio on the Nusselt number at the impingement wall is not very pronounced, as evidenced by the nearly constant average Nusselt number along the impingement wall; see Table 4. When the separation ratio increases from 2 to 5, $\overline{Nu}$ at the impingement wall decreases only 1%. However, the effect of the separation distance on the Nusselt number at the opposite wall is slightly more pronounced, with a decrease of 11% in the average Nusselt number as the separation ratio increases from 2 to 5.

The effect of the offset ratio on the peak Nusselt number at the impingement wall is more pronounced than that of the separation ratio. As the offset ratio increases, for a fixed separation ratio, the maximum Nusselt number decreases and moves downstream with the reattachment point (see Fig. 15). However, despite this decrease in the peak Nusselt number, the average Nusselt number at the impingement wall increases by 20% as the offset ratio varies from 2 to 5 (Table 4). This is due to the slower decrease in the local Nusselt number as the flow develops downstream. At $x/w = 100$, Nu_x at the impingement wall has not yet converged to a value independent of the offset ratio. On the other

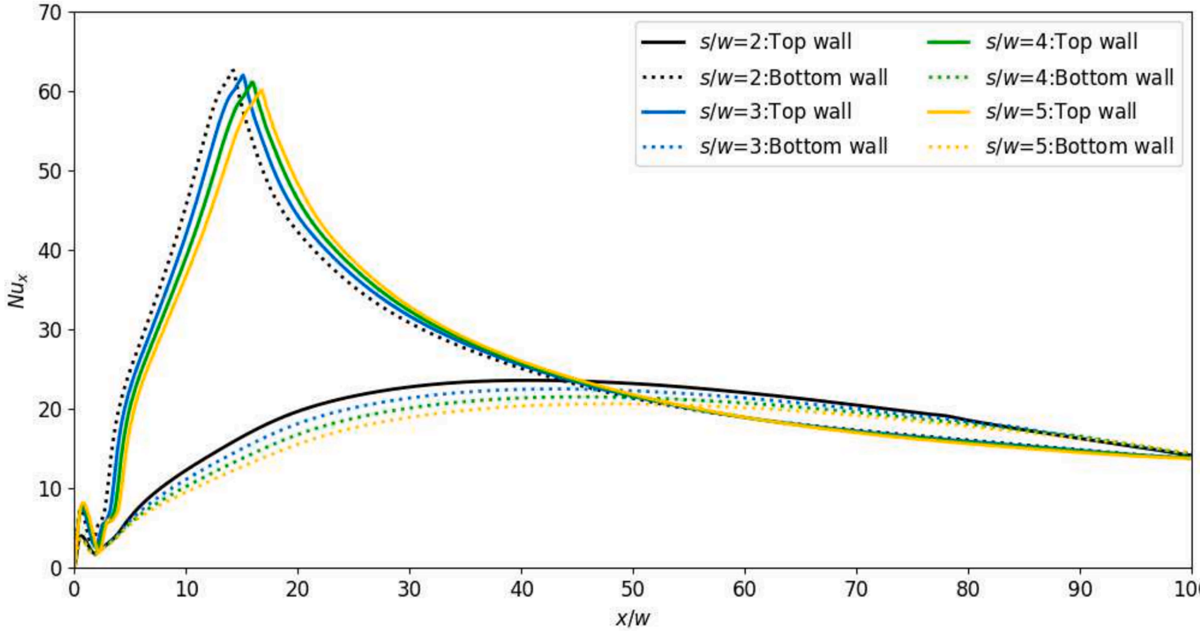

Fig. 22. Local Nusselt number along the bottom and top walls for two confined turbulent plane parallel jets with $h/w = 4$, $Re = 15000$ and several separation ratios.

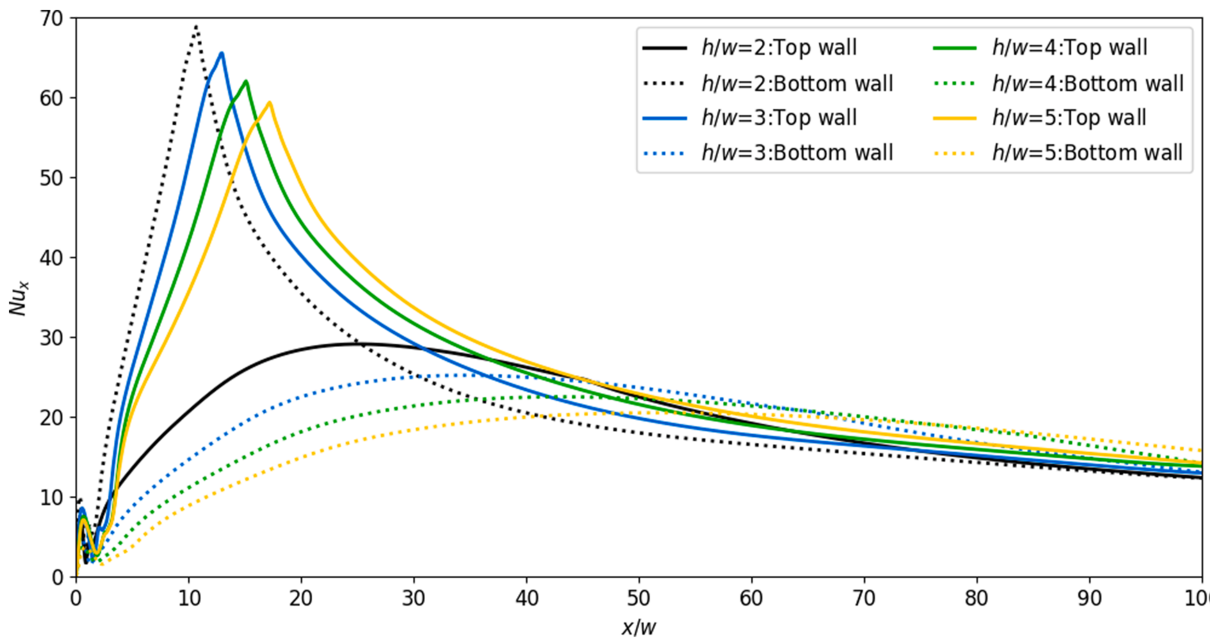

Fig. 23. Local Nusselt number along the bottom and top walls two confined turbulent plane parallel jets with $s/w = 3$, $Re = 15000$ and several offset ratios.

Table 4
Average Nusselt number at the top, $\overline{Nu}_T$, and bottom, $\overline{Nu}_B$, walls for two confined turbulent plane parallel jets with $Re = 15000$ and several separation and offset ratios. The values at the impingement wall are represented in bold.

	s/w			
$h/w = 4$	2	3	4	5
$\overline{Nu}_T$	18.66	**24.57**	**24.47**	**24.34**
$\overline{Nu}_B$	**24.59**	17.94	17.26	16.63
	h/w			
$s/w = 3$	2	3	4	5
$\overline{Nu}_T$	20.00	**23.77**	**24.57**	**27.10**
$\overline{Nu}_B$	**22.60**	19.12	17.94	18.81

hand, as the offset ratio increases, the maximum local Nusselt number on the wall opposite to the jet impingement wall decreases. Accordingly, the average Nusselt number decreases by 10% when h/w is increased from 2 to 4. However, it increases 5% when h/w is increased from 4 to 5.

Eq. (7) and (8) provide correlations for the average Nusselt number as functions of the separation and offset ratios at the impingement wall and the opposite wall, respectively. These correlations were obtained using a least-squares fit and are valid for confined planar dual offset jets with $Re = 15000$, $s/w \in [2, 5]$, and $h/w \in [2, 5]$.

$$\overline{Nu}_{\text{impingement wall}} = 19.65 \left(\frac{h}{w}\right)^{0.183} \left(\frac{s}{w}\right)^{-0.014} \tag{7}$$

$$\overline{Nu}_{\text{opposite wall}} = 23.68\left(\frac{h}{w}\right)^{-0.088}\left(\frac{s}{w}\right)^{-0.124} \tag{8}$$

Both correlations confirm that increasing the separation ratio leads to a decrease in the average Nusselt number on both the impingement and opposite walls, with a more pronounced effect on the opposite wall. In contrast, increasing the offset ratio increases the average Nusselt number at the impingement wall, but decreases it at the opposite wall. Overall, the geometric parameter with the greatest influence on the heat transfer to the impingement wall is the offset ratio, while for the opposite wall, it is the separation ratio.

5. Conclusions

This study investigated the flow physics and heat transfer of heated twin turbulent plane parallel jets confined between isothermal walls using two-dimensional RANS-based CFD simulations. The model was validated against experimental data for both isothermal and non-isothermal jet configurations, and the offset and separation ratios were varied to analyze the effect of these two important parameters on flow behavior and heat transfer. To the best of the authors' knowledge, this study presents the first systematic investigation of the combined effects of these two geometrical parameters in dual plane offset jets.

Despite geometrical symmetry, the jets consistently deflected toward one of the walls due to the Coandă effect, forming stable asymmetric flow structures. This behavior is driven by the low-pressure region near the impingement wall created by asymmetric entrainment. Increasing the separation ratio delays jet merging, shifts the reattachment point downstream, and reduces peak wall shear stress, peak local Nusselt numbers and average Nusselt number along both walls. Higher offset ratios also shift the reattachment point downstream and reduce both peak wall shear stress and peak local Nusselt numbers. However, the average heat transfer at the impingement wall is enhanced by higher offset ratios.

Four turbulence models were tested, with the SST k-ω model providing the most balanced performance across three validation cases involving both isothermal and non-isothermal jets. While RANS models provide efficient tools for parametric analysis, their accuracy depends on the specific flow configuration, and, therefore, generalizations should be made with caution and additional validation against experimental data or higher-fidelity models (e.g., Direct Numerical Simulations) is recommended for flows outside the scope of this study.

Overall, the study contributes to a better understanding of confined turbulent jet systems and offers guidance for optimizing thermal performance in engineering applications such as cooling, combustion, and ventilation.

CRediT authorship contribution statement

Francisco Zdanowski: Writing – review & editing, Visualization, Validation, Software, Methodology, Formal analysis, Data curation, Conceptualization. **Isabel Malico:** Writing – review & editing, Writing – original draft, Validation, Supervision, Resources, Project administration, Methodology, Funding acquisition, Formal analysis, Conceptualization.

Declaration of competing interest

The authors declare that they have no known competing financial interests or personal relationships that could have appeared to influence the work reported in this paper.

Acknowledgements

The authors acknowledge *Fundação para a Ciência e a Tecnologia* (FCT) for its financial support via the project LAETA Base Funding (DOI: 10.54499/UIDB/50022/2020). Additionally, Francisco Zdanowski would like to thank the grant provided by *Fundação para a Ciência e Tecnologia* (reference 2021.04655.BD and DOI: 10.54499/2021.04655.BD).

Data availability

No data was used for the research described in the article.

References

[1] S. Salvador, J.-M. Commandré, Y. Kara, Thermal recuperative incineration of VOCs: CFD modelling and experimental validation, Appl. Therm. Eng. 26 (2006) 2355–2366, https://doi.org/10.1016/j.applthermaleng.2006.02.018.

[2] H. Li, Z. Fu, C. Xi, et al., Study on the impact of parallel jet spacing on the performance of multi-jet stratum ventilation, Appl. Energy 306 (2022) 118135, https://doi.org/10.1016/j.apenergy.2021.118135.

[3] P.J. Murphy, S. Alimohammadi, S.M. O'Shaughnessy, Two-dimensional dual jets—a comprehensive review of experimental and numerical analyses, Energies 17 (2024) 4487, https://doi.org/10.3390/en17174487.

[4] E. Tanaka, The interference of two-dimensional parallel jets: 1st report, experiments on dual jet, Bull JSME 13 (1970) 272–280, https://doi.org/10.1299/jsme1958.13.272.

[5] A. Nasr, J.C.S. Lai, Two parallel plane jets: mean flow and effects of acoustic excitation, Exp. Fluids 22 (1997) 251–260, https://doi.org/10.1007/s003480050044.

[6] E.A. Anderson, R.E. Spall, Experimental and numerical investigation of two-dimensional parallel jets, J. Fluids Eng. 123 (2001) 401–406, https://doi.org/10.1115/1.1363701.

[7] N. Fujisawa, K. Nakamura, K. Srinivas, Interaction of two parallel plane jets of different velocities, J. Vis. 7 (2004) 135–142, https://doi.org/10.1007/BF03181586.

[8] M. Mosavati, R. Balachandar, R.M. Barron, Characteristics of self-oscillating twin jets, Phys. Fluids 33 (2021) 035129, https://doi.org/10.1063/5.0033869.

[9] J.R.R. Pelfrey, J.A. Liburdy, Effect of curvature on the turbulence of a two-dimensional jet, Exp. Fluids 4 (1986) 143–149, https://doi.org/10.1007/BF00280264.

[10] J.R.R. Pelfrey, J.A. Liburdy, Mean flow characteristics of a turbulent offset jet, J. Fluids Eng. 108 (1986) 82–88, https://doi.org/10.1115/1.3242548.

[11] C. Bourque, B.G. Newman, Reattachment of a two-dimensional, incompressible jet to an adjacent flat plate, Aeronaut. Q. 11 (1960) 201–232, https://doi.org/10.1017/S0001925900001797.

[12] R.A. Sawyer, The flow due to a two-dimensional jet issuing parallel to a flat plate, J. Fluid Mech. 9 (1960) 543–559, https://doi.org/10.1017/S0022112060001304.

[13] J. Hoch, L.M. Jiji, Two-dimensional turbulent offset jet-boundary interaction, J. Fluids Eng. 103 (1981) 154–161, https://doi.org/10.1115/1.3240766.

[14] S.H. Yoon, K.C. Kim, D.S. Kim, M.K. Chung, Comparative study of a turbulent wall-attaching offset jet and a plane wall jet, KSME J 7 (1993) 101–112, https://doi.org/10.1007/BF02954360.

[15] A. Nasr, J.C.S. Lai, A turbulent plane offset jet with small offset ratio, Exp. Fluids 24 (1998) 47–57, https://doi.org/10.1007/s003480050149.

[16] S.K. Rathore, M.K. Das, Comparison of two low-Reynolds number turbulence models for fluid flow study of wall bounded jets, Int. J. Heat Mass Transf. 61 (2013) 365–380, https://doi.org/10.1016/j.ijheatmasstransfer.2013.01.062.

[17] T. Mondal, N. Srivastava, S.M. O'Shaughnessy, S. Pramanik, Comparison of the mean flow and turbulence characteristics of a single offset jet and a dual offset jet, Eur. J. Mech. B. Fluids 98 (2023) 161–179, https://doi.org/10.1016/j.euromechflu.2022.12.003.

[18] J.T. Holland, J.A. Liburdy, Measurements of the thermal characteristics of heated offset jets, Int. J. Heat Mass Transf. 33 (1990) 69–78, https://doi.org/10.1016/0017-9310(90)90142-H.

[19] D.S. Kim, S.H. Yoon, D.H. Lee, K.C. Kim, Flow and heat transfer measurements of a wall attaching offset jet, Int. J. Heat Mass Transf. 39 (1996) 2907–2913, https://doi.org/10.1016/0017-9310(95)00383-5.

[20] H.B. Song, S.H. Yoon, D.H. Lee, Flow and heat transfer characteristics of a two-dimensional oblique wall attaching offset jet, Int. J. Heat Mass Transf. 43 (2000) 2395–2404, https://doi.org/10.1016/S0017-9310(99)00312-9.

[21] N. Gao, D. Ewing, C.Y. Ching, Heat transfer in turbulent planar offset attaching jets with small initial offset distances, Int. J. Heat Mass Transf. 83 (2015) 21–26, https://doi.org/10.1016/j.ijheatmasstransfer.2014.11.086.

[22] E. Vishnuvardhanarao, M.K. Das, Computation of mean flow and thermal characteristics of incompressible turbulent offset jet flows, Numer. Heat Transf. A Appl. 53 (2007) 843–869, https://doi.org/10.1080/10407780701715760.

[23] M. Ajmi, N. Hnaien, S. Marzouk, et al., Numerical investigation of heat transfer enhancement of an inclined heated offset jet, Int. Commun. Heat Mass Transf. 116 (2020) 104682, https://doi.org/10.1016/j.icheatmasstransfer.2020.104682.

[24] A.R. Choudhury, K. Anupindi, Large-eddy simulation of a planar offset-jet with heat transfer: the effects of ventilation, Int. J. Heat Mass Transf. 208 (2023) 124061, https://doi.org/10.1016/j.ijheatmasstransfer.2023.124061.

[25] X.K. Wang, S.K. Tan, Experimental investigation of the interaction between a plane wall jet and a parallel offset jet, Exp. Fluids 42 (2007) 551–562, https://doi.org/10.1007/s00348-007-0263-9.

[26] P.J. Murphy, S. Alimohammadi, S.M. O'Shaughnessy, Experimental investigation of a wall-bounded dual jet flow for varying Reynolds number: flow visualisation, hydrodynamic characteristics, and associated heat transfer, Int. J. Therm. Sci. 211 (2025) 109699, https://doi.org/10.1016/j.ijthermalsci.2025.109699.

[27] Z. Li, W. Huai, J. Han, Large eddy simulation of the interaction between wall jet and offset jet, J. Hydrodyn. 23 (2011) 544–553, https://doi.org/10.1016/S1001-6058(10)60148-5.

[28] T. Mondal, M.K. Das, A. Guha, Numerical investigation of steady and periodically unsteady flow for various separation distances between a wall jet and an offset jet, J. Fluids Struct. 50 (2014) 528–546, https://doi.org/10.1016/j.jfluidstructs.2014.07.009.

[29] A. Kumar, Mean flow characteristics of a turbulent dual jet consisting of a plane wall jet and a parallel offset jet, Comput. Fluids 114 (2015) 48–65, https://doi.org/10.1016/j.compfluid.2015.02.017.

[30] T.P. Singh, A. Dewan, Computational study of thermal and fluid mixing behaviour of a dual jet flow using LES approach, Int. Commun. Heat Mass Transf. 154 (2024) 107436, https://doi.org/10.1016/j.icheatmasstransfer.2024.107436.

[31] E. Vishnuvardhanarao, M.K. Das, Study of the heat transfer characteristics in turbulent combined wall and offset jet flows, Int. J. Therm. Sci. 48 (2009) 1949–1959, https://doi.org/10.1016/j.ijthermalsci.2009.02.020.

[32] A. Kumar, Mean flow and thermal characteristics of a turbulent dual jet consisting of a plane wall jet and a parallel offset jet, Numer. Heat Transf. A Appl. 67 (2015) 1075–1096, https://doi.org/10.1080/10407782.2014.955348.

[33] N. Hnaien, S. Marzouk, H.B. Aissia, J. Jay, Wall inclination effect in heat transfer characteristics of a combined wall and offset jet flow, Int. J. Heat Fluid Flow 64 (2017) 66–78, https://doi.org/10.1016/j.ijheatfluidflow.2017.01.010.

[34] P. Murphy, S. Alimohammadi, S. O'Shaughnessy, Experimental analysis of heat transfer to a dual jet flow: effect of Reynolds number, in: 2022 28th International Workshop on Thermal Investigations of ICs and Systems (THERMINIC), IEEE, 2022, pp. 1–6.

[35] P.J. Murphy, S. Alimohammadi, S.M. O'Shaughnessy, Experimental investigation of heat transfer to a dual jet flow with varying velocity ratio, in: 2023 22nd IEEE Intersociety Conference on Thermal and Thermomechanical Phenomena in Electronic Systems (ITherm), IEEE, 2023, pp. 1–8.

[36] T.P. Singh, A. Dewan, A.K. Shukla, Heat transfer enhancement in turbulent dual jet and its thermal characterizations using large eddy simulation, Int. J. Therm. Sci. 192 (2023) 108436, https://doi.org/10.1016/j.ijthermalsci.2023.108436.

[37] P.J. Murphy, S. Alimohammadi, S.M. O'Shaughnessy, Experimental investigation of dual jet flow past a heated surface: effect of Reynolds number, Int. J. Heat Mass Transf. 218 (2024) 124786, https://doi.org/10.1016/j.ijheatmasstransfer.2023.124786.

[38] P.J. Murphy, S. Alimohammadi, S.M. O'Shaughnessy, Experimental investigation of the effect of the offset ratio on the flow characteristics and heat transfer behaviour of a wall-bounded dual jet flow, Int. J. Thermofluids 26 (2025) 101125, https://doi.org/10.1016/j.ijft.2025.101125.

[39] T. Mondal, S. Pramanik, Numerical study on mean flow field of turbulent dual offset jet, Proc Inst Mech Eng C 235 (2021) 6865–6882, https://doi.org/10.1177/09544062211000774.

[40] T. Mondal, S.M. O'Shaughnessy, Numerical investigation of conjugate heat transfer to a turbulent dual offset jet, Int. J. Therm. Sci. 180 (2022) 107716, https://doi.org/10.1016/j.ijthermalsci.2022.107716.

[41] A. Nasr, J.C.S. Lai, Comparison of flow characteristics in the near field of two parallel plane jets and an offset plane jet, Phys. Fluids 9 (1997) 2919–2931, https://doi.org/10.1063/1.869404.

[42] A. Assoudi, N. Mahjoub Saïd, H. Bournot, G. Le Palec, Comparative study of flow characteristics of a single offset jet and a turbulent dual jet, Heat Mass Transf. 55 (2019) 1109–1131, https://doi.org/10.1007/s00231-018-2493-1.

[43] M.R. Boroomand, A. Mohammadi, Investigation of k-ε turbulent models and their effects on offset jet flow simulation, Civ Eng J 5 (2019) 127, https://doi.org/10.28991/cej-2019-03091231.

[44] V.M. Behera, S.K. Rathore, Heat transfer augmentation by plate motion in a wall jet flow over a heated plate: a conjugate heat transfer technique, Numer. Heat Transf. A Appl. 85 (2024) 2280–2297, https://doi.org/10.1080/10407782.2023.2220906.

[45] A.I. Zografos, W.A. Martin, J.E. Sunderland, Equations of properties as a function of temperature for seven fluids, Comput. Methods Appl. Mech. Eng. 61 (1987) 177–187, https://doi.org/10.1016/0045-7825(87)90003-X.

[46] F.R. Menter, Two-equation eddy-viscosity turbulence models for engineering applications, AIAA J. 32 (1994) 1598–1605, https://doi.org/10.2514/3.12149.

[47] ANSYS, Inc, Ansys Fluent Theory Guide. ANSYS, Inc., Canonsburg, PA., 2024.

[48] I.B. Celik, U. Ghia, P.J. Roache, et al., Procedure for estimation and reporting of uncertainty due to discretization in CFD applications, J. Fluids Eng. 130 (2008) 078001, https://doi.org/10.1115/1.2960953.

[49] ANSYS FLUENT software. https://www.ansys.com/products/fluids/ansys-fluent. Accessed 25 Mar 2025.

[50] N. Hnaien, S. Marzouk, L. Kolsi, et al., Numerical study and correlations development on twin-parallel jets flow with non-equal outlet velocities, Front Heat Mass Transf 11 (2018), https://doi.org/10.5098/hmt.11.8.

[51] B.E. Launder, D.B. Spalding, The numerical computation of turbulent flows, Comput. Methods Appl. Mech. Eng. 3 (1974) 269–289, https://doi.org/10.1016/0045-7825(74)90029-2.

[52] V. Yakhot, S.A. Orszag, Renormalization group analysis of turbulence. I. Basic theory, J Sci Comput 1 (1986) 3–51, https://doi.org/10.1007/BF01061452.

[53] B.E. Launder, G.J. Reece, W. Rodi, Progress in the development of a Reynolds-stress turbulence closure, J. Fluid Mech. 68 (1975) 537–566, https://doi.org/10.1017/S0022112075001814.

[54] B.E. Launder, B.I. Sharma, Application of the energy-dissipation model of turbulence to the calculation of flow near a spinning disc, Lett. Heat Mass Transfer 1 (1974) 131–138, https://doi.org/10.1016/0094-4548(74)90150-7.

[55] Z. Yang, T.H. Shih, A new time scale based k-ε model for near-wall turbulence, AIAA J. 31 (1993) 1191–1198, https://doi.org/10.2514/3.11752.

[56] S.K. Rathore, M.K. Das, A comparative study of heat transfer characteristics of wall-bounded jets using different turbulence models, Int. J. Therm. Sci. 89 (2015) 337–356, https://doi.org/10.1016/j.ijthermalsci.2014.11.019.

[57] F.R. Menter, Review of the shear-stress transport turbulence model experience from an industrial perspective, Int. J. Computat. Fluid Dyn. 23 (2009) 305–316, https://doi.org/10.1080/10618560902773387.

[58] H. Li, N.K. Anand, Y.A. Hassan, Computational study of turbulent flow interaction between twin rectangular jets, Int. J. Heat Mass Transf. 119 (2018) 752–767, https://doi.org/10.1016/j.ijheatmasstransfer.2017.12.008.